Author's Accepted Manuscript

www.elsevier.com/locate/ijmactool

A review of geometrical and microstructural size effects in micro-scale deformation processing of metallic alloy components

M.W. Fu, J.L. Wang, A.M. Korsunsky

PII: S0890-6955(16)30085-2
DOI: http://dx.doi.org/10.1016/j.ijmachtools.2016.07.006
Reference: MTM3178

To appear in: *International Journal of Machine Tools and Manufacture*

Received date: 23 April 2016
Revised date: 10 July 2016
Accepted date: 19 July 2016

Cite this article as: M.W. Fu, J.L. Wang and A.M. Korsunsky, A review of geometrical and microstructural size effects in micro-scale deformatio processing of metallic alloy components, *International Journal of Machine Tool and Manufacture,* http://dx.doi.org/10.1016/j.ijmachtools.2016.07.006

A review of geometrical and microstructural size effects in micro-scale deformation processing of metallic alloy components

M.W. Fu[a*, c], *J.L. Wang*[a], *A. M. Korsunsky*[b#]

[a] Department of Mechanical Engineering, The Hong Kong Polytechnic University, Hung Hom, Kowloon, Hong Kong

[b] Multi-Beam Laboratory for Engineering Microscopy (MBLEM), Department of Engineering Science, University of Oxford, Parks Rd, Oxford OX1 3PJ, U.K.

[c] PolyU Shenzhen Research Institute, No. 18 Yuexing Road, Nanshan District, Shenzhen, PR China

Corresponding Emails:

* Email: mmmwfu@polyu.edu.hk; Tel:852-27665526

Email: alexander.korsunsky@eng.ox.ac.uk; Tel: +44 1865 2 73043

Abstract

Plastic deformation at the macroscopic scale has been widely exploited in industrial practice in order to obtain desired shape and control the requested properties of metallic alloy parts and components. The knowledge of deformation mechanics involved in various forming processes has been systematically advanced over at least two centuries, and is now well established and widely used in manufacturing. However, the situation is different when the physical size of the workpiece is scaled down to the micro-scale (μ-scale). In such cases the data, information and insights from the macro-scale (m-scale) deformation mechanics are no longer entirely valid and fully relevant to μ-scale deformation behavior. One important reason for the observed deviation from m-scale rules is the ubiquitous phenomenon of Size Effect (SE). It has been found that the geometrical size of workpiece, the microstructural length scale of deforming materials and their interaction significantly affect the deformation response of μ-scale objects. This observation gives rise to a great deal of research interest in academia and industry, causing significant recent effort directed at exploring the range of related phenomena. The present paper summarizes the current state-of-the-art in understanding the geometrical and microstructural SEs and their interaction in deformation processing of μ-scale components. The geometrical and grain SEs in μ-scale deformation are identified and articulated, the manifestations of the SE are illustrated and the affected phenomena are enumerated, with particular attention devoted to pointing out the differences from those in the corresponding m-scale domain. We elaborate further the description of the physical mechanisms underlying the phenomena of interest, viz., SE-affected deformation behavior and phenomena, and the currently available explanations and modeling approaches are reviewed and discussed. Not only do the SEs and their interaction affect the deformation-related phenomena, but they also induce considerable scatter in properties and process performance measures, which in turn affects the repeatability and reliability of deformation processing. This important issue has become a bottleneck to the more widespread application of μ-scale deformation processing for mass production of μ-scale parts. What emerges is a panoramic view of the SE and related phenomena in μ-scale deformation processing. Furthermore, thereby the outstanding issues are identified to be addressed to benefit and promote practical applications.

Keywords: Size effect, μ-scaled plastic deformation, Property and performance scatter, Uncertainty Quantification

1. Introduction

With the increasing demand for micro-scale (μ-scale) parts and components in connection with product miniaturization in microelectronics, biomedical engineering, and consumables industries, the spotlight of attention and development effort has once again fallen on manufacturing technology, at the μ-scale in particular. Several generic approaches can be identified to producing miniature, or μ-scale parts and components. One approach is the Micro-Electro-Mechanical Systems (MEMS) manufacturing methods, such as X-ray lithography [1, 2], ink-jet printing [3], etc. Another is mechanical-based μ-manufacturing processes that include μ-machining [4, 5], μ-injection molding [6-8], powder injection molding [9, 10], and μ-forming [11-13].

Micro-forming (μ-forming) is a prominent manufacturing technology for fabricating μ-scale parts with at least two dimensions less than one millimeter. μ-forming can be used to produce bulk (approximately equiaxed) parts, or to produce components that are thin in one dimension using sheet metal (foil) as initial material form. Fig.1 shows some μ-scale parts made by μ-forming processes. μ-forming has some clear advantages, such as high productivity, low-cost, ability to fabricate complex geometries, extensive range of materials to which the methods can be applied, superior mechanical properties of the finished product, and the net-shape or near net-shape fabrication capability [14]. μ-forming, however, also has some inherent disadvantages, such as challenges in the manipulation of billets and preforms in between different processing operations, and the ejection of the final formed part from the die cavity, as well as the fluctuation of dimensional accuracy, geometry rendering, and property variability due to the inhomogeneous and random nature of grain distribution and orientation, referred to in this paper as process performance scatter.

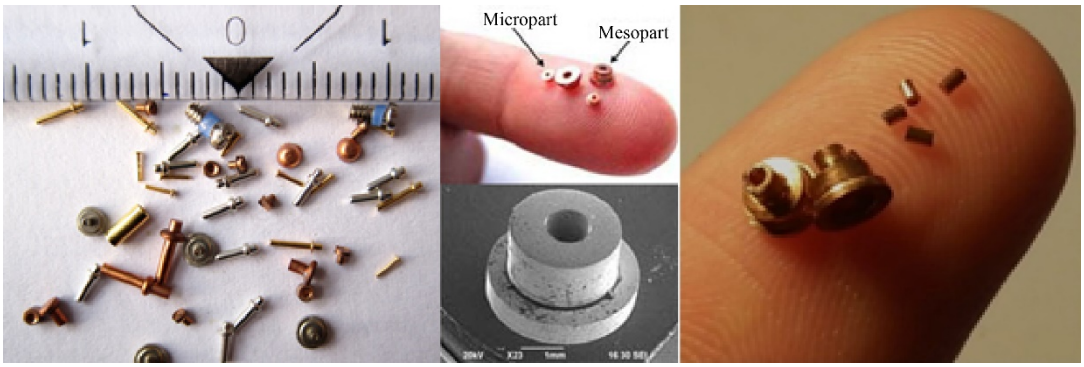

Fig. 1. Industrial μ-parts.

The principles and theory of μ-forming processing are based on the μ-scale plastic deformation analysis. While the conventional m-scale material properties, flow behavior, formability, fracture behavior and friction in plastic deformation processing are well understood and are routinely practiced by the industrial community to provide solutions for part design, process configuration, parameter specification, tooling development, and product quality control and assurance [15, 16], these existing approaches cannot be applied directly to μ-scale deformation processes, since the emergence of the so-called size effect (SE) impedes direct transfer of methodology from m-scale to μ-scale [17-19].

Comprehensive research activities conducted in the past two decades were aimed at elucidating different aspects of the problem, such as the influence of plastic deformation on the apparent SE(s), the elucidation of the underlying physical mechanisms and advanced numerical modeling of μ-scale deformation, process development and optimization, and the assessment of performance and quality of μ-scale parts. Reported investigations of SE-related material behavior are partially listed in Fig.2 and include studies of SE manifestations in the flow stress [17, 20, 21], fracture behavior [22-27], flow behavior [28], elastic recovery [29-31], frictional behavior [32], surface roughening [33-35], and the hardness of μ-formed parts [36, 37]. The mechanisms underlying these SEs were investigated through simulation using the surface layer model [11, 38], mixed material model [39], composite constitutive model [40, 41], etc. These modeling

approaches were proposed in order to describe quantitatively the consequences of SEs on the μ-scale deformation parameters, such as the force, temperature, strain rate and die geometry required for optimum outcomes. In respect of μ-forming processing quality, the influence of SEs on the dimensional accuracy [29, 42, 43], the occurrence of deformation defects [44-47], product mechanical properties [48, 49], and surface finish [50, 51] of μ-formed parts are reviewed.

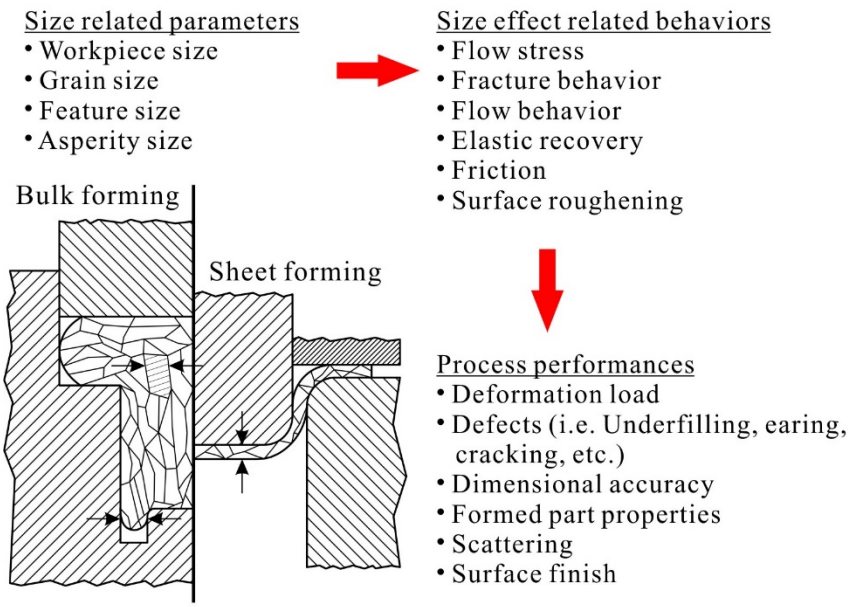

Fig. 2. Graphical illustration of SE related issues in μ-forming processes [13].

Although studies of μ-scale deformation behavior of materials have been conducted over several decades, and the modeling approaches incorporating SEs have been developed, many unknowns and uncertainties persist in relation to SEs. Significant challenges remain, e.g. predicting material deformation behavior at correct scale, enhancing the performance of μ-scale deformation processing, improving the mechanical properties of μ-formed parts and the quality of tooling, and optimizing process parameters.

This paper is distinct from previous reviews of μ-forming and the associated size effects (SEs) in that it introduces a systematic approach to the identification of the underlying origin of SE as a transition between two asymptotes of behavior, each dominated by a single specific physical

mechanism. This fundamental view serves as a generic basis for treating such phenomena as elastic springback in μ-forming, grain size effect, etc. The same approach is adopted in presenting a comprehensive review of research publications devoted to SEs in μ-scale deformation processing. Firstly, the fundamentals of SEs in the strength of solid materials and structures are introduced and explained. Next, a systematic classification is presented related to the deformation behavior affected by SE and how these differ from m-scale deformation. The existence and characteristics of this aspect of μ-scale deformation in terms of elastic recovery, material flow irregularity, flow stress, fracture behavior, frictional phenomenon and surface roughening are reviewed and summarized. In addition, the physical mechanisms and modeling approaches are presented, and their limitations are identified. These unique aspects of deformation behavior lead to the uncertainty of μ-scale deformation and give rise to performance scatter that has become an issue of concern since it affects significantly the repeatability and reliability of the process, presenting a challenge to quality assurance and control in terms of dimensional accuracy and property variation of manufactured parts. As a guideline, identical material, tooling setting and μ-forming systems can give rise to about 20% performance scatter in terms of the required deformation load and part dimensional accuracy. Addressing this issue is sought to pave the way for more reliable mass production of μ-parts using μ-scale deformation processing. The final part of the paper addresses the underlying issues related to the understanding of μ-deformation mechanics and mechanisms, and to the promising large-scale applications of μ-manufacturing processing. Throughout the paper, state-of-the-art in research is reviewed. The authors' insights are systematically presented with the overall intention to provide a panoramic view of the SE and related phenomena, to improve the performance of μ-forming, and to contribute to strengthening the μ-manufacturing discipline within the context of mechanical and manufacturing engineering science.

2. The fundamentals of the SE in the deformation and strength of solids

2.1. Discussion on the sources of SEs

Various types of SE can be identified by considering the physical mechanism interactions that give rise to them, as explained in the following section. Some authors previously attempted to classify these related phenomena according to density, shape (geometry) and microstructure, respectively, as shown in Fig. 3. However, this classification does not appear complete: in considering μ-forming operations it is necessary to add a class of SEs related to strain gradient phenomena and tribological effects, such as surface roughness and friction. Furthermore, a unified basis for SE description is proposed, and its application to the existing observations is illustrated.

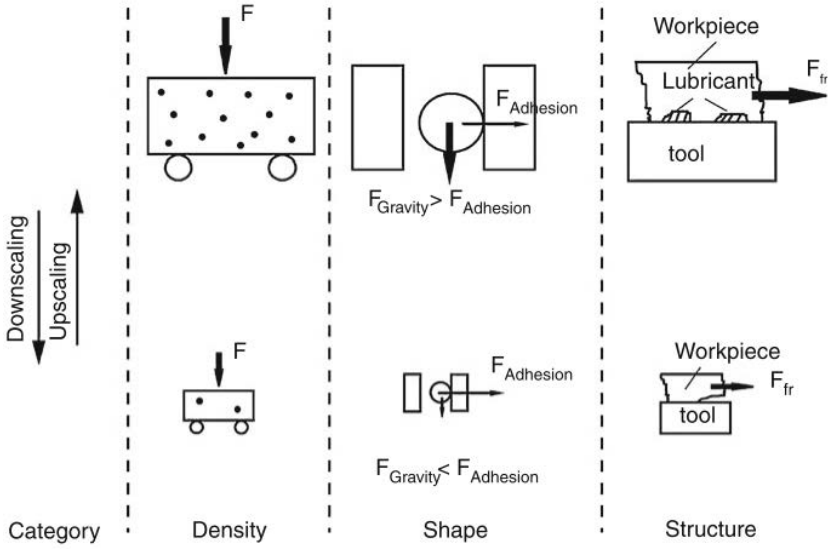

Fig. 3. Graphical illustration of three types of SEs [52].

2.2. Power law scaling

We begin the analysis of SEs by reviewing some fundamental scientific facts that underlie this subject of study. Following Bazant (2002) [53], we establish the fact that when the strength (flow stress, forming load, etc.) of a system is governed by single physical mechanism, the dependence

of this strength measurement on the physical size of the system *must* obey a power law. This rule can be referred to as the *theorem of power law scaling of strength*.

To prove this theorem, it needs to first consider a family of geometrically and structurally identical physical systems differing only in size, subjected to tests to evaluate their strength, Y, as a function of the characteristic size of the structure, D. Let strength values Y_0, Y_1 and Y be found for the structures of size D_0, D_1 and D, respectively. In accordance with the theory of dimensionless analysis, the strength dependence on size must be given solely by a function of the size ratio, $\lambda = D/D_0$:

$$Y / Y_0 = f(D / D_0) = f(\lambda). \tag{1}$$

Since none of these geometrically similar structures can be preferred, it makes no difference which pair of objects to choose for substitution into this expression (D and D_0, or D and D_1), so that the following relations also hold:

$$Y_1 / Y_0 = f(D_1 / D_0), \qquad Y / Y_1 = f(D / D_1). \tag{2}$$

From the three relations above it follows that:

$$\frac{f(D / D_0)}{f(D_1 / D_0)} = f(D / D_1). \tag{3}$$

To solve this functional equation for the unknown scaling law $f(\lambda)$, we differentiate it with respect to D, and substitute $D_1 = D$, leading to the differential equation

$$\frac{D}{D_0} f'\left(\frac{D}{D_0}\right) = f'(1) f\left(\frac{D}{D_0}\right), \quad \text{or} \quad \lambda f'(\lambda) = f'(1) f(\lambda). \tag{4}$$

Introducing the notation $f'(\lambda) = m$, the equation can be rewritten in a variable separable form,

$$\frac{df}{f} = m\frac{d\lambda}{\lambda}. \tag{5}$$

Solving it with the obvious initial condition, $f(1)=1$ and giving the only solution for function f, there exists the following power law:

$$f(\lambda) = \lambda^m, \quad \text{or} \quad Y = Y_0\left(\frac{D}{D_0}\right)^m = CD^m. \tag{6}$$

This establishes a general result of very wide applicability:

In the absence of a characteristic length, the strength (or, indeed, any other similar physical parameter) of a structure scales with its size according to a power law.

This argument can be extended to the description of the material stress-strain dependence by noting that strain itself represents a dimensionless combination of the maximum extension ΔD (that could be considered to be fixed in a mechanical test) and the original length, i.e. sample dimension D.

An alternative way of expressing Eq. (6) is to use what might be called "the Griffith sense", by which the critical condition for failure is written in the form of expression that equates the combination of loading parameter (force Y in the present example) and sample geometry (size D) to a strength-related material property as follows:

$$Y\ D^{-m} = C. \tag{7}$$

For example, in the case of fracture toughness failure criterion in the Linear Elastic Fracture Mechanics (LEFM) context, $Y = \sigma_f$, which is the failure stress, D is the crack half-length, $m = -1/2$, and $C = K_{Ic}/\sqrt{\pi}$, where K_{Ic} is the plane strain fracture toughness.

Power law scaling of strength and deformation parameters is omnipresent in the phenomenological laws describing the mechanical behavior of materials. Several examples are listed in Table 1. It is important to note that, despite the power law exponents appearing in each of these laws being different, none of these laws is referred to as 'SEs', precisely for the reason that the simple power law relationship persists right across the full range of geometric dimensions.

Table 1. Power law scaling in the context of material strength

Hooke's law	$\sigma = E\varepsilon$
Power law plasticity	$\sigma = k\varepsilon^n$
Power law creep	$\frac{d\varepsilon}{dt} = A\sigma^n$
Paris law of fatigue crack growth	$\frac{da}{dN} = A\Delta K^n$
Kachanov's law of damage accumulation	$\frac{d\omega}{dt} = C\omega$

In terms of the underlying physical mechanisms that govern the material deformation response, each of the instances of pure power law behavior corresponds to a situation when a single physical mechanism persists, and no characteristic length scale is present. Conversely, if a characteristic length of some kind arises, then all structures can no longer be thought of as indistinguishable, and strength scaling may obey some more complex function. It is this situation that has become known as the SE.

2.3. Mechanism interactions, scaling transitions and SEs

Let us now address a situation when two distinctly different physical mechanisms determine the deformation response of materials. For the purpose of general analysis the dependence on sample size and strain can be thought of as closely linked: if the final component shape is

prescribed, then, for example, the workpiece thickness directly determines the maximum strain caused within it during deformation.

To introduce the concept of mechanism interaction and scale transition let us consider elasto-plastic deformation with power law hardening that is conveniently described by the Ramberg-Osgood constitutive law:

$$\varepsilon = \frac{\sigma}{E} + \left(\frac{\sigma}{K}\right)^n, \tag{8}$$

where ε and σ are true strain and true stress, respectively, E is Young's modulus, and K and n are the hardening modulus and power law exponent, respectively. The Ramberg-Osgood relation expresses a fundamental fact that total true strain can be decomposed additively into elastic and plastic strain contributions. It also indicates that there is a competition between two physical mechanisms of deformation, namely, the elastic and plastic response. Due to the power exponent $n > 1$ at the small value of σ, the total strain is determined by the elastic strain. At the large strain, on the other hand, the plastic part of strain dominates. The interaction and competition between the two distinct mechanisms of deformation leads to a "crossover" between the two power law trends illustrated in Fig.4, in which the Ramberg-Osgood relation is plotted as normalized strain *vs* normalized stress using logarithmic scale. The normalization is performed here with respect to the crossover values defined by the point at which the two strain contributions are equal, i.e.

$$\frac{\sigma_0}{E} = \left(\frac{\sigma_0}{K}\right)^n, \text{ and hence } \sigma_0 = \left(\frac{K^n}{E}\right)^{1/(n-1)}. \tag{9}$$

The crossover strain therefore is found to be

$$\varepsilon_0 = \left(\frac{K}{E}\right)^{n/(n-1)}. \tag{10}$$

It is clear that for $\varepsilon/\varepsilon_0$ much smaller than unity ($\varepsilon/\varepsilon_0 \ll 1$) the material response is dominated by elasticity, and by plasticity for $\varepsilon/\varepsilon_0$ much greater than unity ($\varepsilon/\varepsilon_0 \gg 1$). The crossover strain defines the condition around which the stress-strain dependence deviates from a simple power law, and a more complex model is required to capture the behavior correctly. This is a manifestation of the SE. It lends itself to a description of the transition using the so-called "knee function" introduced and described in [54].

In practice there is a further characteristic strain and stress values that limit the power law dominance under large deformation. Indeed, the above description of material deformation can be used until an implicit assumption holds of homogeneity of strain distribution within the sample. This is limited by the onset of instability known as "necking", when localization of tensile strain leads to the reduction of cross-sectional area that occurs faster than strain hardening, leading to the loss of load-bearing capacity, and failure.

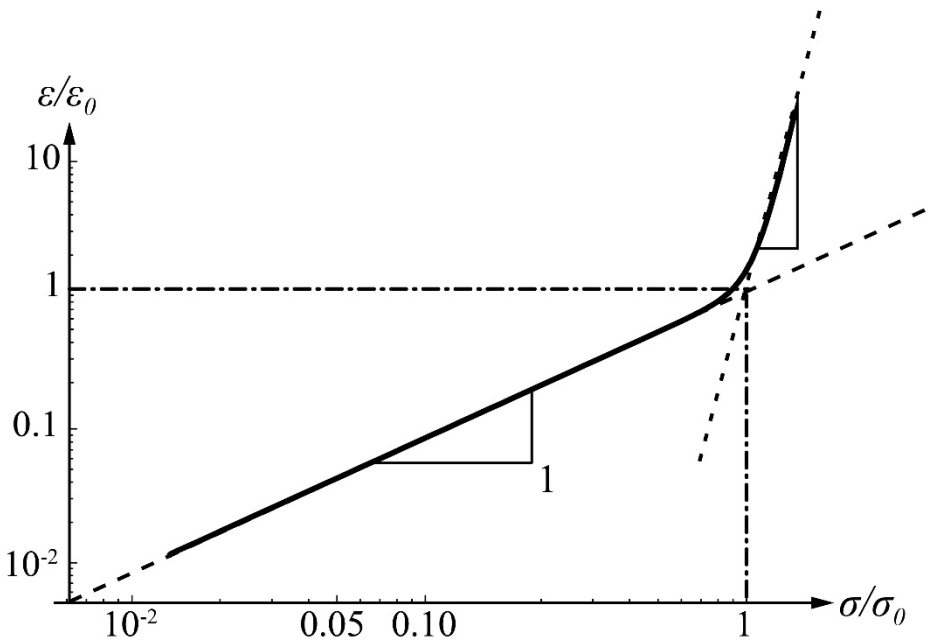

Fig. 4. The power law crossover in the Ramberg-Osgood relation plotted as normalized strain *vs* normalized stress as a manifestation of the SE.

The onset of necking can be described by the condition of the maximum engineering stress being reached, described graphically by the Considère's construction, and expressed algebraically by the relation $\mathrm{d}\sigma / \mathrm{d}\varepsilon = \sigma$. For large deformation, the elastic strain contribution can be ignored, so that using only the plastic strain with power law hardening, $\sigma = K\varepsilon^{1/n}$, it leads to the characteristic strain for plastic instability and onset of failure: $\tilde{\varepsilon} = 1/n$. This strain value sets the limit on the applicability of power law strain hardening response.

In summary, deformation SEs occur as a consequence of the interaction and competition between different physical mechanisms that lead to the appearance of characteristic crossover values of strain, or other dimensionless parameters that describe sample geometry and properties. It is on this basis that the various manifestations of SE can be considered, as discussed below.

3. SE-affected deformation behavior in μ-scale deformation

3.1. Deformation behavior

The previous section introduced fundamental insights into the origins of the SE that can be traced back to the interaction and competition between different physical mechanisms governing the material deformation response, and the characteristic length scales that represent boundaries between distinct “simple” deformation regimes.

Key length scales can be identified that arise as a consequence of transition between deformation mechanisms in microstructured materials:

- Grain size, *d*, is the linear dimension of material volumes of persistent regular crystal lattice characterized by anisotropic elasticity, and plastic deformation mediated by crystal slip or twinning.
- Strain gradient plasticity length scale, *l*, arises as a consequence of dislocation structuring to accommodate inhomogeneous deformation (geometrically necessary dislocations, or GND, according to Ashby [55]).

- Smallest linear dimension of the sample that is closest in scale to other characteristic length scales determines many aspects of sample response to forming. This allows distinguishing between *sheet forming*, where the smallest sample dimension is t, the sheet or foil thickness, and bulk forming, where the sample is approximately equiaxed, and sample diameter D plays the role of its key geometric dimension.
- A measure of surface roughness, r, affects many aspects of the interaction between forming die and sample, and determines the formation of near surface boundary layers caused by friction effects.

We begin with the discussion of the way in which the relationship between the specimen size and grain size affects the material flow behavior in μ-scale plastic deformation processing. To study the specimen SE on material flow behavior, Chan et al. [33] conducted a series of upset forging experiments using cold drawn and annealed pure copper billets of different sizes from m- to μ-scale. Images of specimens after compression are shown in Fig. 5, which shows the cross-sections of compressed specimens changing in shape from circular to irregular with the decreasing sample diameter and increasing grain size. A similar observation was found in compression of Al AA6061 cylinders with different sizes, as shown in Fig.6. Deformation inhomogeneity is clearly more severe in the case of coarse-grained samples, or, to be more precise, with increasing ratio of grain size to sample diameter, d/D. The irregular shape of deformed specimens is caused by the random variation in grain shape, size and orientation. Grain level deformation occurs by crystal slip on the selected slip systems (defined by the slip plane normal and the slip direction) determined by the combination of grain orientation and applied stress, in accordance with Schmid law [56]. Slip most readily occurs on close-packed planes (i.e. planes that have the greatest number of atoms per unit area, and hence the largest distance from the parallel plane of the same kind), and in close-packed directions (i.e. directions in which the distance between atoms is smallest, making each individual slip "jump" the shortest). Since each crystallite (grain) has several equivalent slip systems, the slip system(s) activated are the one(s) with the largest driving force

expressed by the resolved shear stress, and the lowest resistance, known as the critical resolved shear stress (CRSS). m-scale polycrystalline samples typically contain great numbers of grains that are randomly and evenly distributed within samples. Even though significant contrast in properties exists between grains, it does not affect the overall response due to effective overall averaging. Similarly, the large difference between sample dimension and grain size means that deformation mechanisms remain consistent between different sample sizes, and no SE can be seen. However, when the specimen size is scaled down to become comparable to the grain size, this leads to only a few grains of material spanning the entire sample width, so that the deformation of each grain exerts a significant influence on the overall sample deformation. Strain differences between neighboring grains need to be accommodated by grain boundary sliding, leading to surface roughening. In summary, when the properties of each grain begin to play a significant role in the overall deformation response, inhomogeneous deformation and significant scatter in response may arise, depending on specific sample structure. SEs on deformation behavior become apparent as the material changes from polycrystal to oligocrystal (i.e. few-grained) with decrease of the ratio of specimen size to grain size [57].

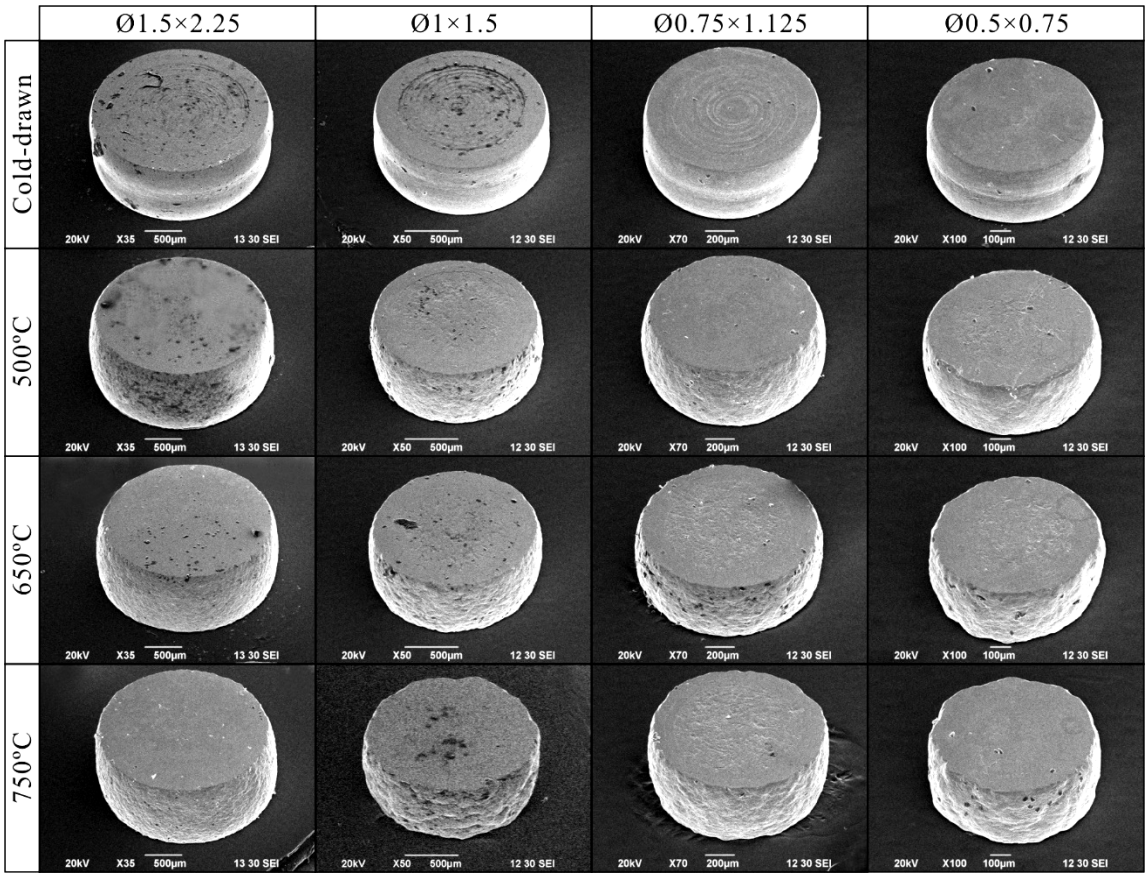

Fig. 5. Scanning electron microscope photographs of the compressed samples (unit: mm) [33].

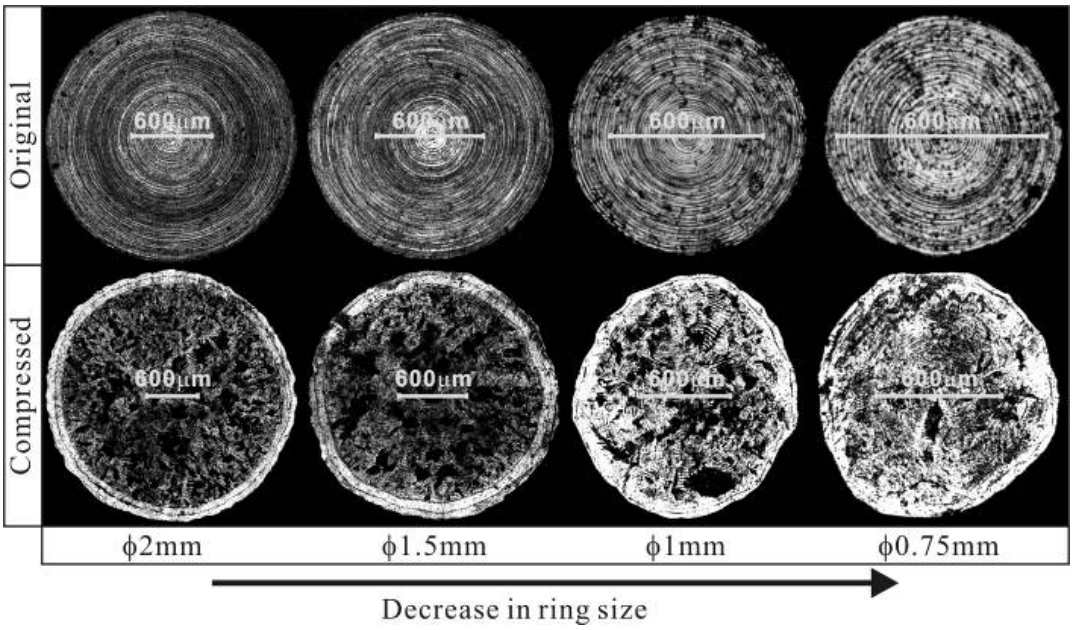

Fig. 6. Cross-sectional photographs of the initial and compressed samples [57].

In μ-scale deformation processing, the quality of the μ-formed part is a critical issue. The main issues of concern include the geometrical accuracy of μ-formed parts since dimensional precision down to sub-millimeter or even to a few microns is required for many industrial applications, and ensuring the production of defect-free μ-parts and the high durability and reliability of the designed μ-forming system.

In the sections below we focus attention on some further specific aspects of deformation behavior and the manifestation of SEs.

3.2. Elastic recovery

As becomes evident from the Ramberg-Osgood additive representation of strain, any forming operation that involves the application of load and generation of stress within the workpiece gives rise to both elastic and plastic strains. Considering sheet metal forming as an example, the elastic strain corresponds to the recoverable part of deformation that leads to the so-called springback behavior after the removal of external load. The value of springback depends on the elasto-plastic characteristics of the workpiece material and reduces the dimensional accuracy of the formed μ-parts. The springback behavior has been investigated in various experiments. L-bending using steel and copper alloy strips was conducted in the lead frame production process and it was found that springback decreases with die radius, die angle and the clearance between punch and die. And the results also show that springback angle along the rolling direction is bigger than that in the transverse direction [42]. Through another L-bending experiments using a range of pure copper foils of different thicknesses but with similar microstructure, the influence of SEs on springback was studied, and the scatter in the springback angle for coarse-grained material is larger than fine-grained one, due to the increasing influence of each grain on the deformation process [20]. Furthermore, the increasing surface grains causing a reduction in the springback angle exerts an influence that is countered by the strain gradient effect, causing an increase in springback angle. In summary, it can be concluded that the springback angle decreases with the foil thickness down

to a certain thickness $t_0 \approx 100\mu m$, as shown in Fig.7. Once the influence of surface grains becomes dominant, the springback angle increases with further decrease of foil thickness. In addition, three-point bending of copper foils was used to study the interaction between geometrical and grain sizes and the results showed that springback angle does not vary monotonously with the thickness to grain size ratio, *t*/*d* (thickness ratio, for short) [30]. For the small thickness ratios (typically, foil thickness less than 0.4mm), the springback angle increases with the decreasing *t*/*d* ratio. However, when the thickness ratio becomes larger (typically, for thickness larger than 0.4mm), the springback angle increases with increasing sheet thickness. The elastic anisotropy of surface grains due to the grain size and random orientation lead to the complex variation of springback behavior. Similar conclusions were obtained using brass foils [29, 31].

The above-mentioned research stated that contrary influence of SEs and strain gradient effect on springback behavior, however, the physical mechanism behind this phenomenon is need to be furtherly explored and how SEs and strain gradient effect in-turn affect springback should be deeply investigated.

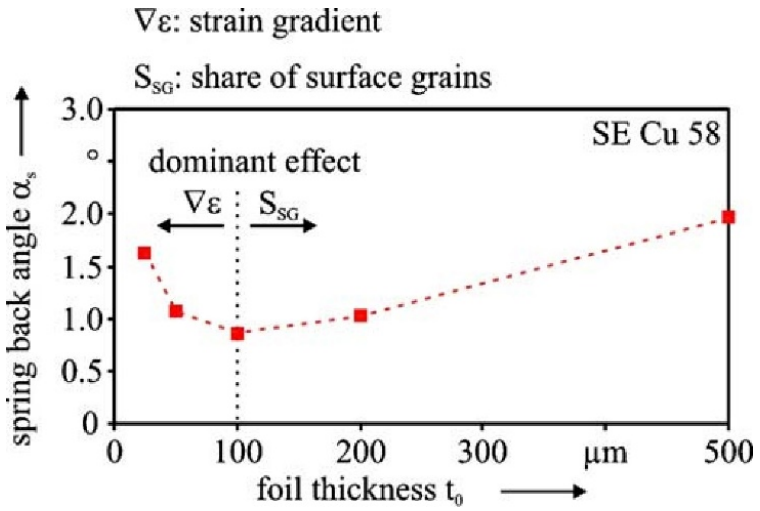

Fig. 7. Springback angle as a function of the foil thickness *t* [20].

3.3. Material flow irregularities

Similar to macroscopic deformation processes, forming defects may arise as a consequence of material flow irregularities in meso- and μ-scale deformation processes. Flow-induced defects correspond to one of the most common problems in μ-formed parts, as in other bulk forming processes. Since components with forming defects often give rise to sudden failure in service, defect formation mechanisms must be investigated and avoided in early design stage. Typical flow-induced defects are the folding in material flow and the unfilling in some places in die cavity. The folding defect in bulk forming processes refers to the undesirable meeting of material flows in opposite directions and forming new contacting surfaces via merging of the unreasonable material flows in the deformation body. Fig.8 shows the occurrence of folding defects in both m- and μ-scale flanged parts. Extrusion experiments in meso-scale were conducted to investigate the formation mechanism of flow-induced defects [46]. By using a non-axisymmetric part with 2D axisymmetrical features with flow-induced defects as case, it was found that the undesirable flow patterns and deformation modes result in the formation of folding defects, as shown in Fig. 9. To support up-front design and reveal the root-causes of the defect, a feature-based method was developed to determine the best forming sequences for defect-free parts in meso- and μ-scale deformation processes, and a defect-free multi-stage forming process was figured out. The main rationale of the feature-based method is to identify the features with flow-induced defects and then to form these features first with defect-free.

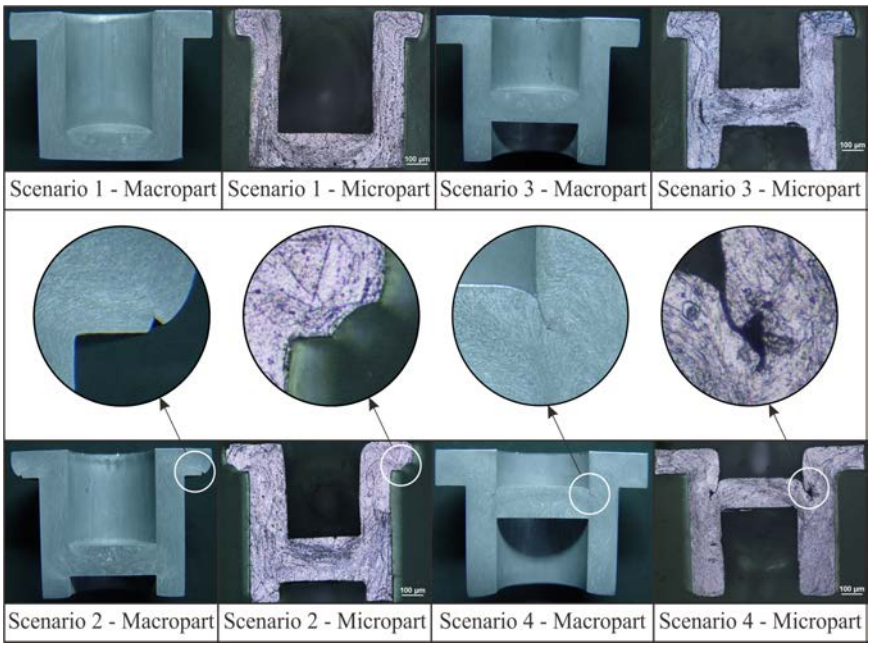

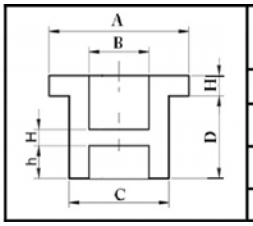

Design scenario	Macropart						Micropart					
	A	B	C	D	H	h	A	B	C	D	H	h
1	35	15	25	20	5	0	1	0.43	0.71	0.57	0.14	0
2	35	15	25	20	5	3.75	1	0.43	0.71	0.57	0.14	0.11
3	35	15	25	20	5	7.5	1	0.43	0.71	0.57	0.14	0.21
4	35	15	25	20	5	15	1	0.43	0.71	0.57	0.14	0.43

Fig. 8. m- and μ-scale axisymmetric flanged parts and the occurrence of flow-induced defects in both m- and μ-scales (unit: mm) [58].

From material flow perspective, the flowability is deteriorated when the geometry of workpiece is scaled down due to the increase of friction in between the tooling and material. Fig.8 also shows the defects became worse in μ-scale deformation.

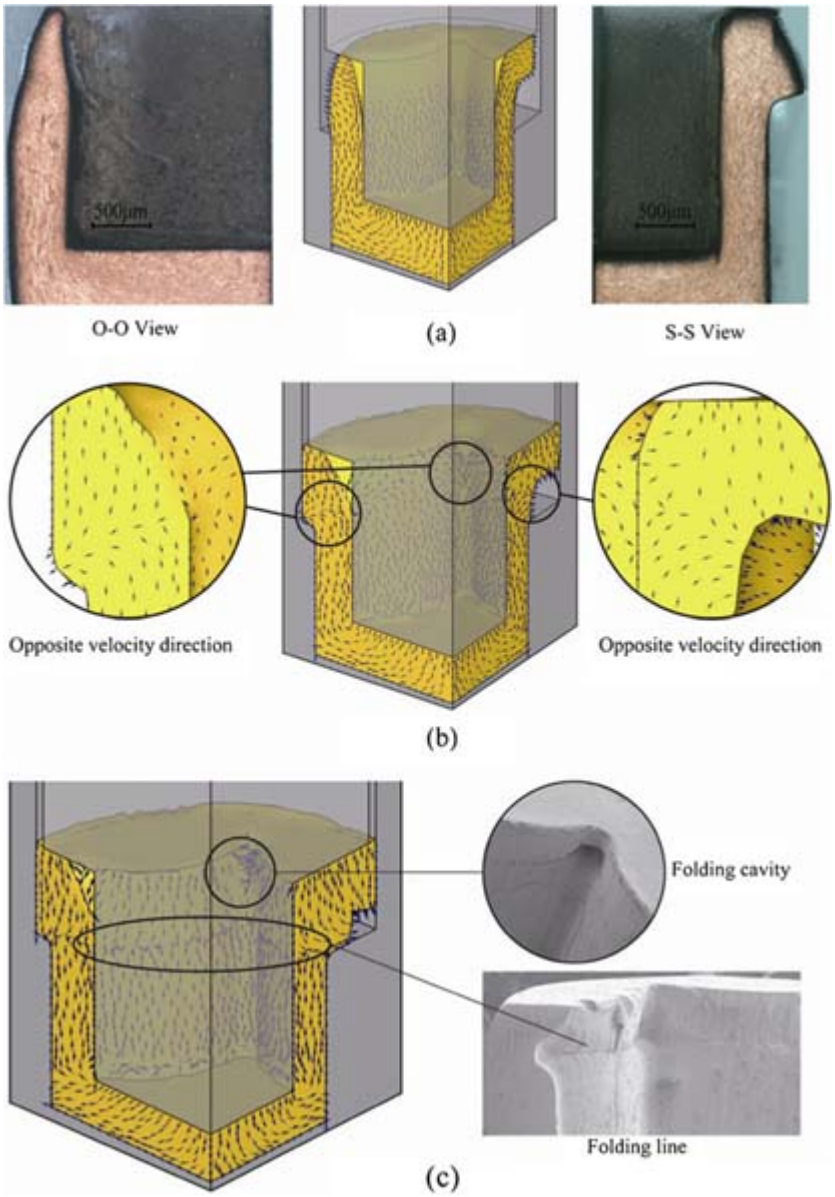

Fig. 9. Formation process of folding defects at the stroke of (a) 75 %, (b) 90 %, and (c) 95 %. [46].

3.4. Flow stress

Flow stress is the instantaneous stress required to deform the material, i.e. history-dependent yield strength for inelastic deformation that determines the material resistance to forming (shape change) by plastic flow. This parameter affects both the choice of processing conditions and design of tooling, and the mechanical properties of μ-formed parts. The SE on flow stress has been extensively investigated by scaling down standard tests while monitoring the influence of

different features and grain sizes, with the results reported in prior arts [57, 59-63]. The dependence of flow stress-strain relationship on the sample and grain sizes of several alloys is illustrated in Fig. 10. In this case, the flow stress increases with the sample size and decreases with the increasing grain size. The grain SE on flow stress is significant for both m- and μ-sized samples, while the SE of sample geometry only becomes significant when less than 10 grains are present in the cross-section of sample [12]. Several notable studies reported in the field of sheet metal forming, including CuZn35 alloy sheet of different thickness [31], pure copper [64] and aluminum alloy samples [60]. SE on flow stress has also been studied for bulk processing in compression tests with pure copper, C3602 brass, and Al 6061 alloy similarly scaled samples [27, 33, 57].

The reduction of flow stress with the decreasing of geometry size of sample can be explained by the so-called surface layer model. The surface grains of sample experience less deformation constraints compared to the interior grains of material, resulting in the surface grains exhibiting a lower flow stress [14] and thus the flow stress of the samples decreases with the increase of surface grain percentage in the samples with small geometry size.

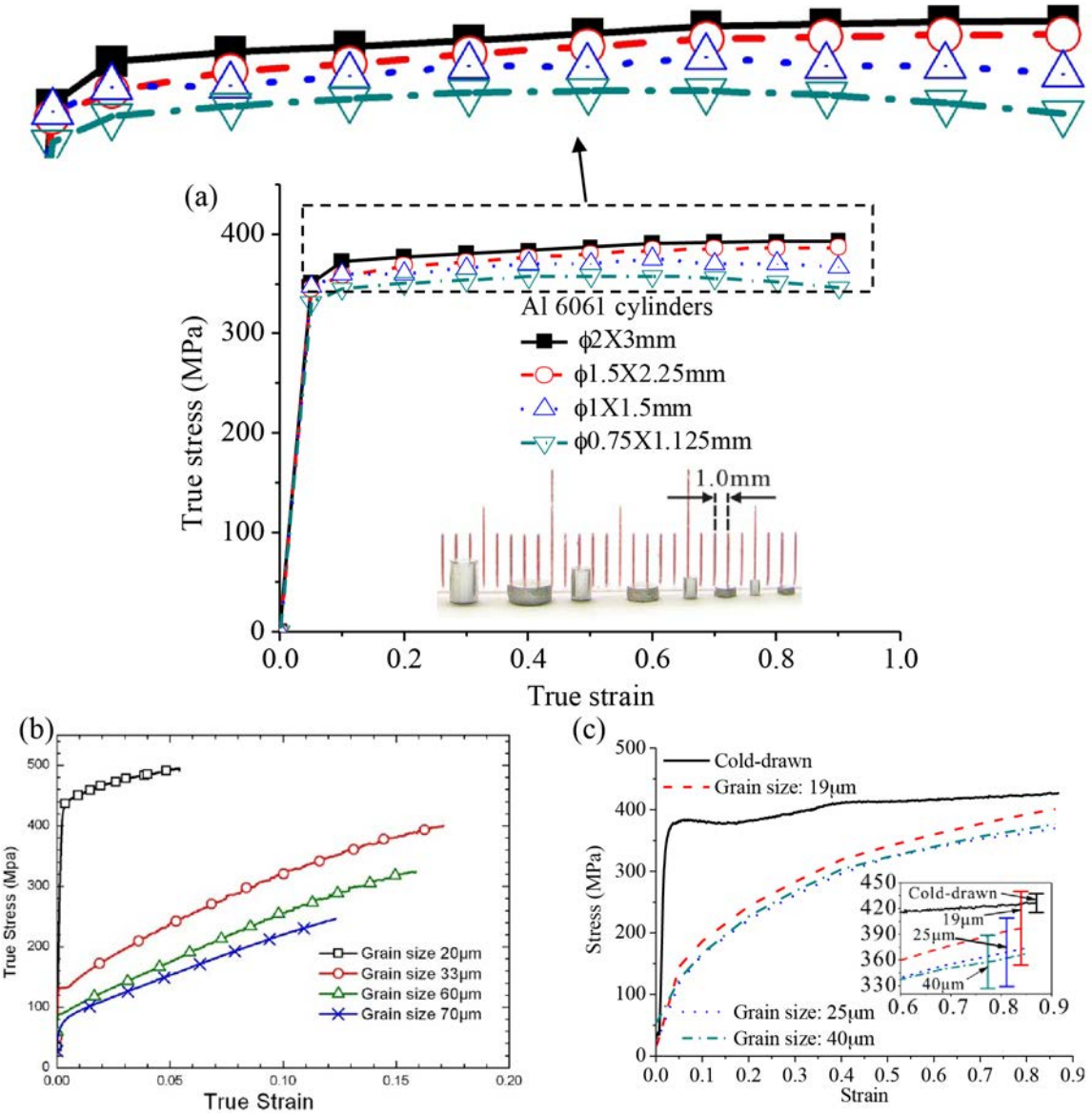

Fig. 10. Influence of grain and geometry SEs on flow stress. (a) Compression stress-strain curves of Al 6061 samples with different geometry sizes [57]. (b) Tensile test results of the thin samples of CuZn35 alloy with different grain sizes (t=0.1 mm) [31], and (c) Compression tests conducted on the small samples of C3602 brass with the diameter of 0.5mm and the length of 0.75mm [33].

3.5. Fracture behavior

In bulk μ-scale deformation process, the volume of workpiece plays a more significant role compared with sheet μ-scale forming where the influence of workpiece surface prevails. To explore the SE on fracture behavior in μ-scale bulk forming, the flanged upsetting using brass

C3602 was conducted [27]. It was found in Fig. 11 that formability decreases with the increase of specimen size for a given grain size. In other words, the material is able to undergo larger plastic deformation before initiation of fracture in μ-scale deformation. It was also believed that the damage energy to initiate fracture in μ-scale deformation is the same as that in m-scale. Therefore, in order to reach the critical damage energy, the material with smaller flow stress can undergo a larger strain in μ-scale deformation.

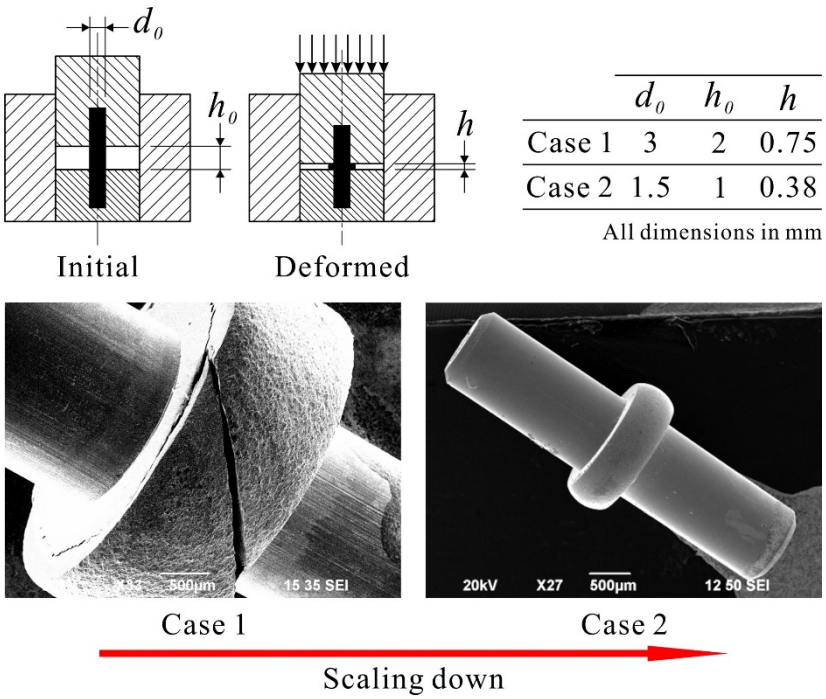

Fig. 11. Comparison of deformation response of centrally headed parts with different geometry sizes [27].

In sheet metal μ-scale deformation process, Fig. 12 shows that the variation of fracture strain with the ratio of sheet thickness to grain size (t/d) in uniaxial tensile tests [22, 24, 26] and the fracture strain decreases rapidly when t/d ratio is less than 12 [65]. From SEM fractography in Fig. 13, it can be seen that the amount of microvoids seen at the fracture region decreases with the t/d ratio [66].

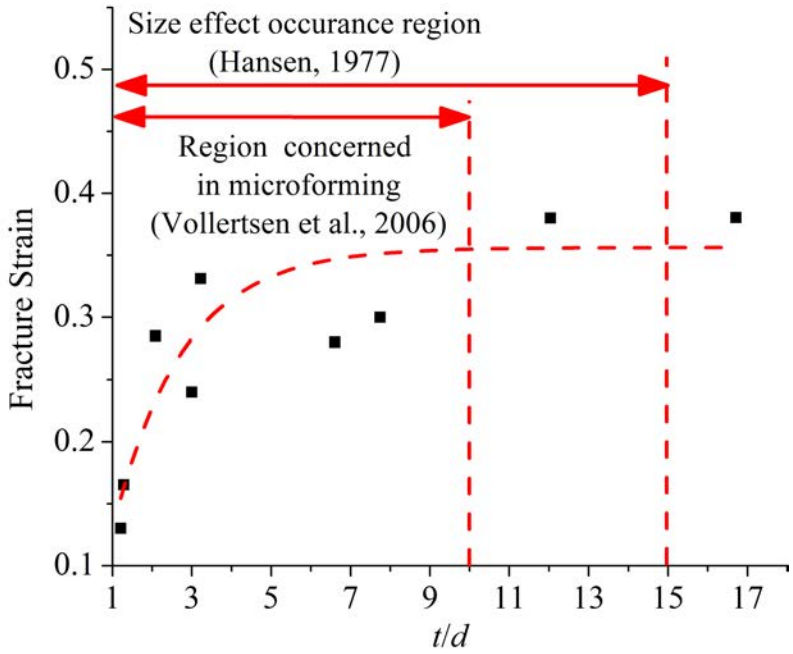

Fig. 12. Change of fracture strain with the thickness to grain size (*t/d)* ratio [26]. The dashed trend line is provided as a guide to the eye.

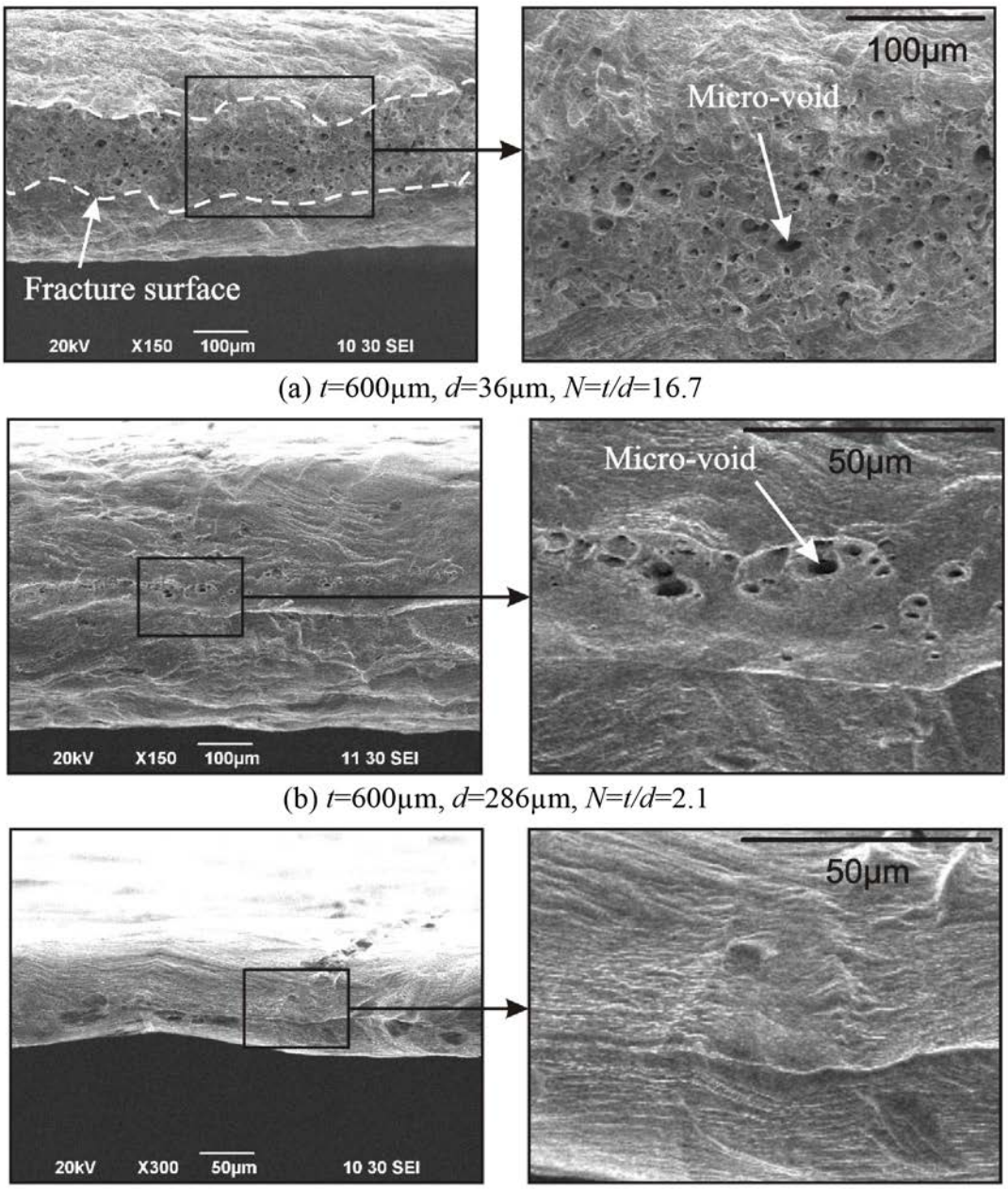

Fig. 13. Fractography of tested samples [26].

3.6. Frictional phenomena

Two approaches can be found in literature to investigating SEs on friction in μ-scale deformation. One involves the size-scaled ring compression test [17], and the other is the double cup extrusion (DCE) test [14], which involves higher surface expansion and pressure, and thus represents more closely practical situation encountered in bulk μ-scale deformation [67-69]. The friction is determined through measurement of the change of the shape and dimensions of the

deformed sample. For the former, the inner diameter of the deformed ring decreases with the increasing friction, while for DCE, the ratio of upper cup height h_u to lower cup height h_l increases with the friction [14], as illustrated in Fig.14. DCE was conducted using specimen with scaled down diameters in the range 4.8–0.5 mm. It was found that μ-scaling led to a significant increase in friction with decreasing specimen size.

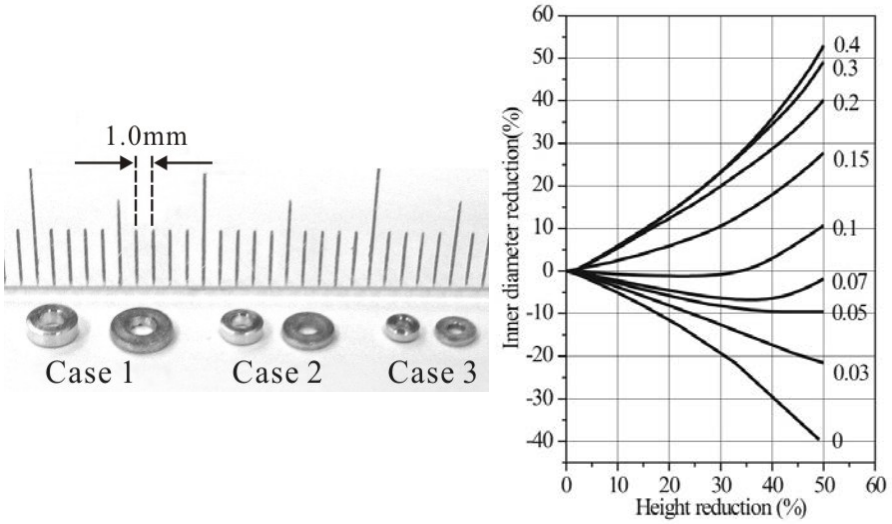

(a) Ring compression test [57]

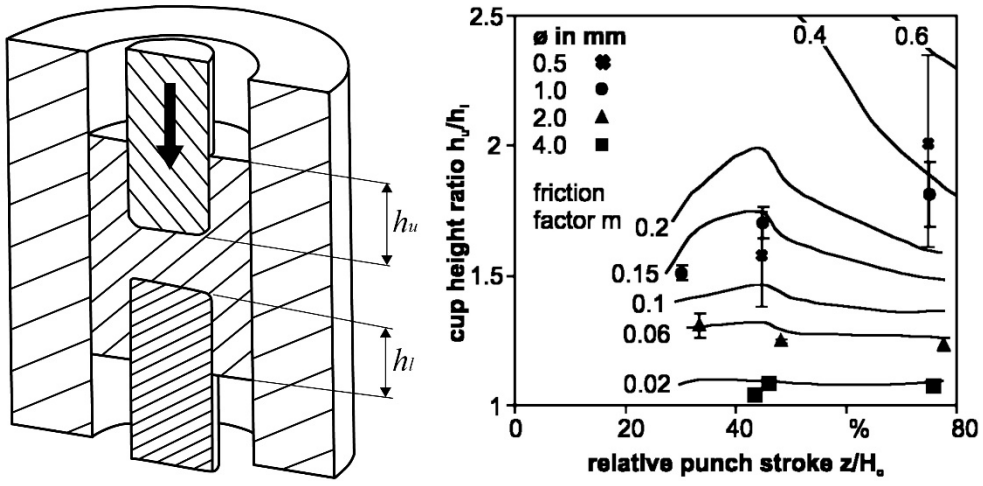

(b) Formed sample geometries obtained in differently scaled double cup extrusion tests [14].

Fig. 14. Measurement of friction coefficient by experiment

For dry frictional condition, the observed relationship between interfacial friction and SE is more contradictory. Some researches show no SE in μ-scale deformation [70-72]. There is thus

no unambiguous conclusion regarding the influence of specimen size on the interfacial friction under dry condition. Furthermore, the mechanism and physics behind those observed phenomena need to be explored and investigated further. From methodological perspective the above-mentioned two approaches are generally used for m-scaled deformation, but their use for μ-scale deformation needs to be validated.

3.7. Surface roughening

Surface roughening is known to increase with grain size in forming operations. The level of the surface roughening becomes severe as the geometrical size is decreased down to the μ-scale. This is associated with plastic deformation being mediated by dislocations that self-organize into slip bands, which are sensitive to the anisotropic elasto-plastic deformation at the grain level. At the microscopic scale, the anisotropy of grain level deformation, including surface grains, results in differences in the out-of-plane displacements that manifest themselves as surface roughness. Furthermore, the surface grains experience less constraint, so that strain incompatibility between neighboring grains can be accommodated by local extrusion at sample surface, causing further inhomogeneity of profile. The extent of roughening is affected by the crystal structure [73]. Greater roughening occurs for the materials with crystal structures that have a low number of slip systems available, such as the hexagonal close-packed (hcp) structure. When only a few slip systems can accommodate local deformation, strain incompatibility is exacerbated, and leads to the increased surface roughening. Additionally, plastic deformation is confined by the neighboring grain boundaries, causing slip lines, as shown in Fig. 15.

The deformation interaction between neighboring grains can be classified into three categories graphically described in Fig. 16. The case of relatively large deformation taking place in only one of the grains is shown in Fig. 16a. Fig. 16b shows deformation in both grains and the grain boundary may correspond to a band of modified strain distribution, and Fig. 16c introduce no visible disturbance.

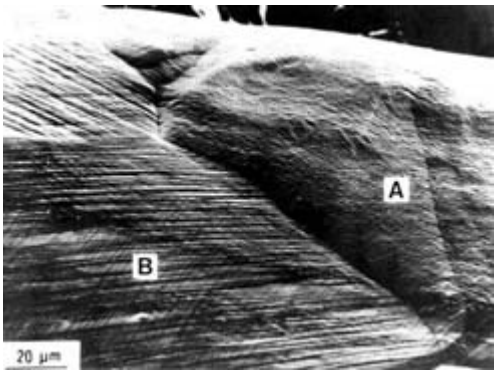

Fig. 15. SEM image of a deformed aluminum polycrystal [74].

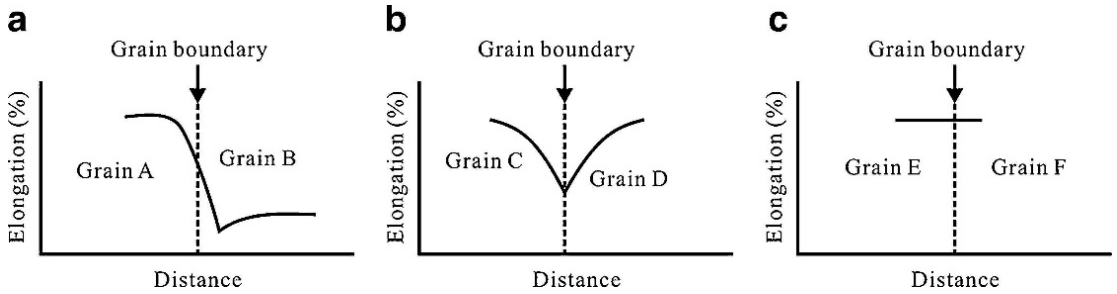

Fig. 16. Schematic diagrams of three types of deformation profiles near a grain boundary [75].

In the context of studying bulk μ-scale deformation processes, upsetting experiments on pure copper for different billet sizes and grain sizes were performed to investigate the influence of SE on the evolution of surface roughness [33]. Fig.17 shows SEM images of surface topography of μ-heading specimens. It is found that surface roughness increases with grain size [76-82]. Free surface roughening of copper sheet in uniaxial tension shown in Fig.18 [83] increases significantly with the decrease of the t/d ratio. Fig. 19 shows the dependence of surface roughness of stretched foils of different thicknesses and grain size measured by profilometry [35].

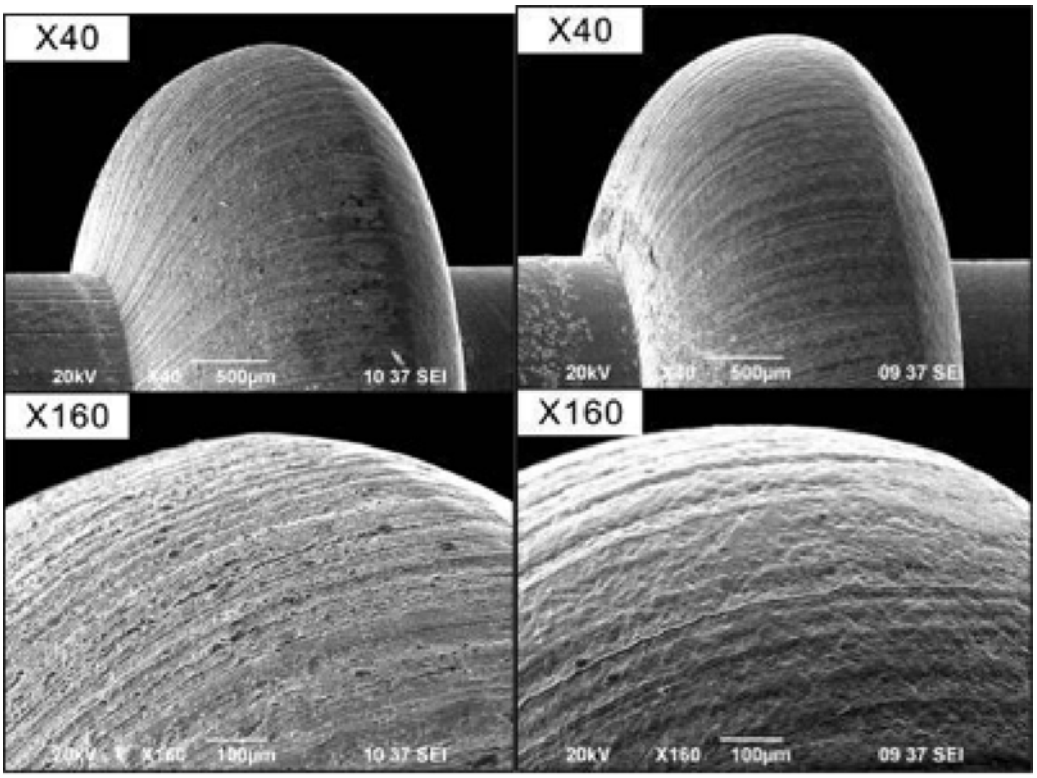

(a-1) Cold-drwan (a-2) Grain size: 26μm

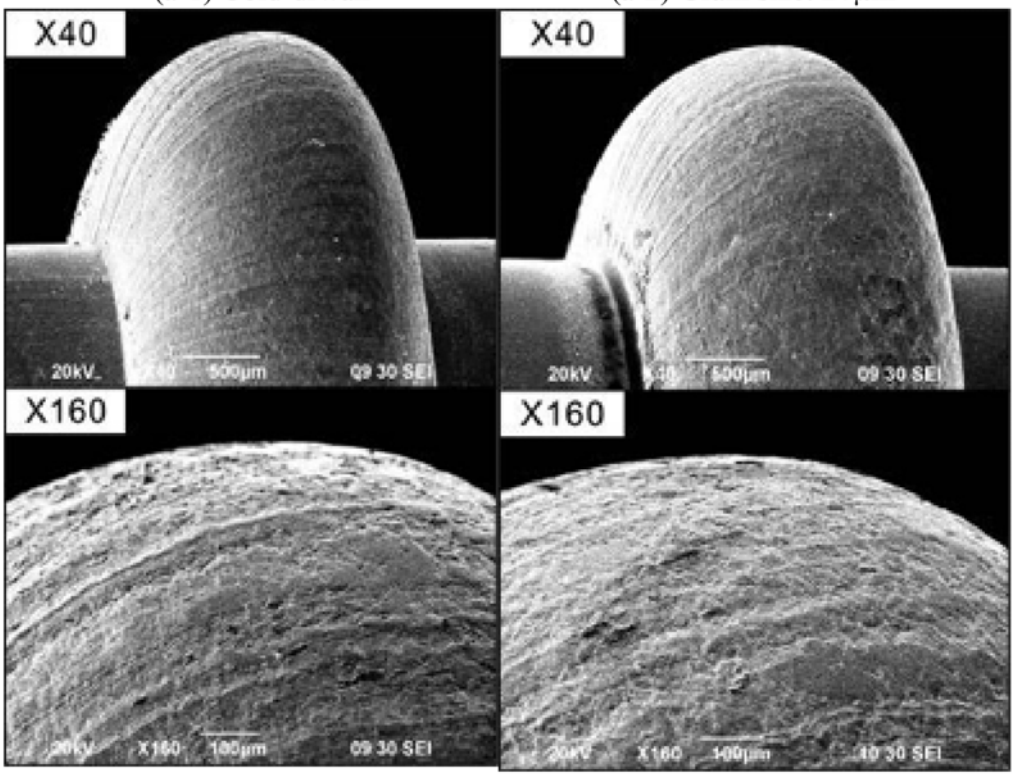

(a-3) Grain size: 38μm (a-4) Grain size: 50μm

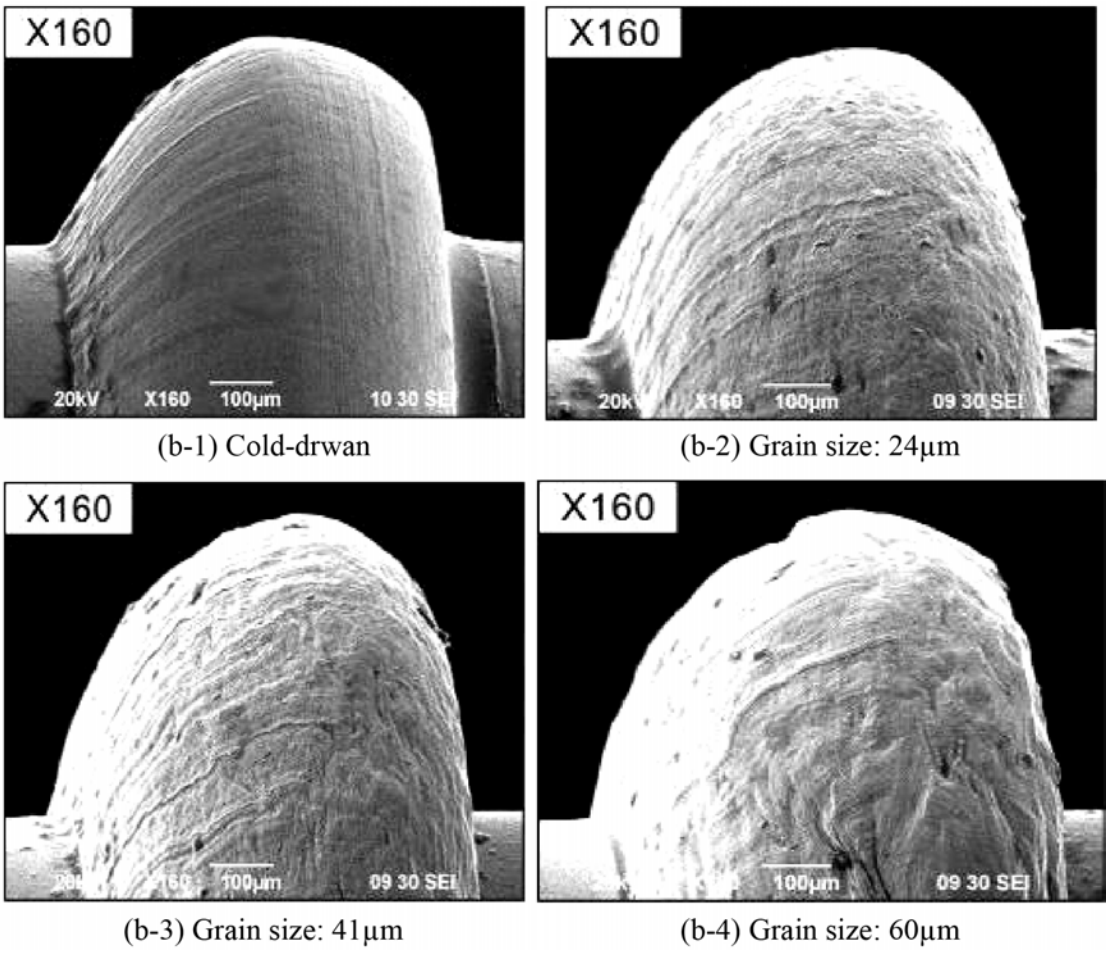

Fig. 17. SEM images illustrating the surface topography of µ-heading specimens of (a) macroscopic size, and (b) microscopic size for different material conditions [35].

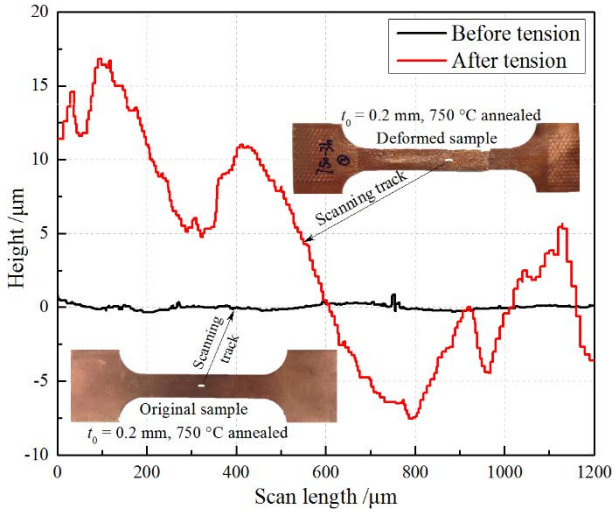

Fig. 18. Illustration of the free surface roughening phenomenon of pure copper sheets after tensile test [83].

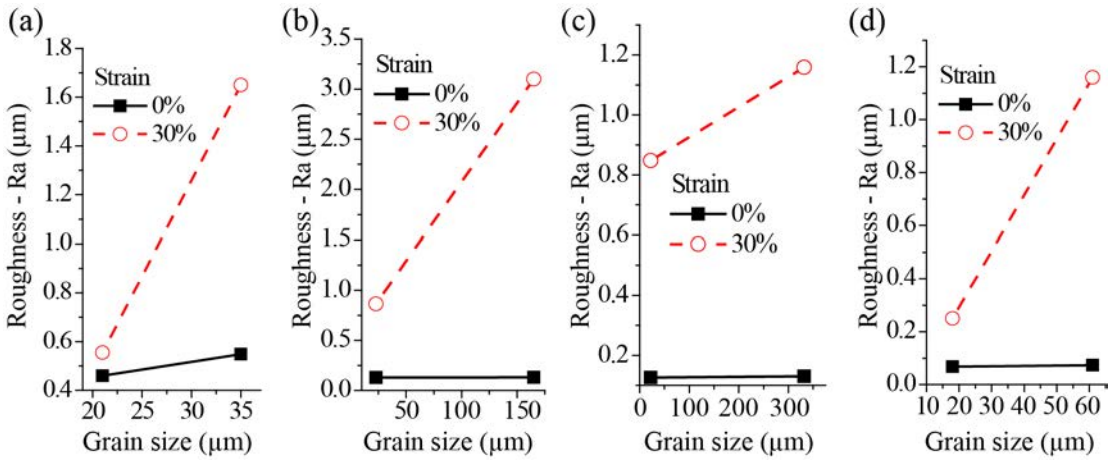

Fig. 19. The variation of surface roughness with grain size for the samples with different thicknesses: (a) t=100 μm , (b) t=400 μm, (c) t= 600 μm, and (d) t=1500 μm [35].

In order to improve the performance of μ-scale forming process, vibration-assisted method, which has been proven to be able to improve formability in m-scale forming process, could be used in μ-scale. Ultrasonic vibration is exerted on tooling and could reduce deformation load and obtain better surface finish of μ-formed parts. In addition, authors also suggest that increasing forming temperature a certain level such as to warm forming temperature would facilitate more uniform material flow to get a better surface roughness.

4. SE mechanisms and modeling

4.1. Surface layer model

The influence of SEs on the overall load required to deform the sample (also is referred to as the flow stress) can be explained by the so-called surface layer model [14]. The outer surface grains of material are less constrained than the grains lying within its bulk. Whereas dislocations moving through a grain lying close to the free surface may emerge at the surface, in bulk grains, however, they pile up at grain boundaries [84-86]. This leads to lower hardening and lower flow stress in surface grains. With the decreasing geometrical size (more specifically, with the smaller

thickness to grain size ratio, *t*/*d*), the share of surface grains increases, leading to a lower overall flow stress. The overall apparent flow stress of a μ-sized workpiece can be determined by the combination of contributions from the surface and interior grains [39, 87, 88]. The decrease in the overall flow stress can therefore be attributed to the increase of fraction of surface grains. This relationship is formulated as:

$$\sigma(\varepsilon)=\eta\sigma_s(\varepsilon)+(1-\eta)\sigma_i(\varepsilon) \tag{11}$$

where $\sigma_s(\varepsilon)$ and $\sigma_i(\varepsilon)$ are the flow stresses of surface and internal grains, respectively, that are thought to be the function of strain experienced at these locations, and $\eta=V_s/(V_s+V_i)$ is the volume fraction of surface grains.

In fine-grained macroscopic samples, the volume fraction of surface grains is small such that the interior grain behavior determines the overall response. However, when the workpiece is scaled down to μ-scale, the grain size remains relative large and only a few grains find themselves located within the interior of the material. The volume fraction of surface grains thus increases considerably and shown in Fig.20. This results in the decrease of the apparent overall flow stress.

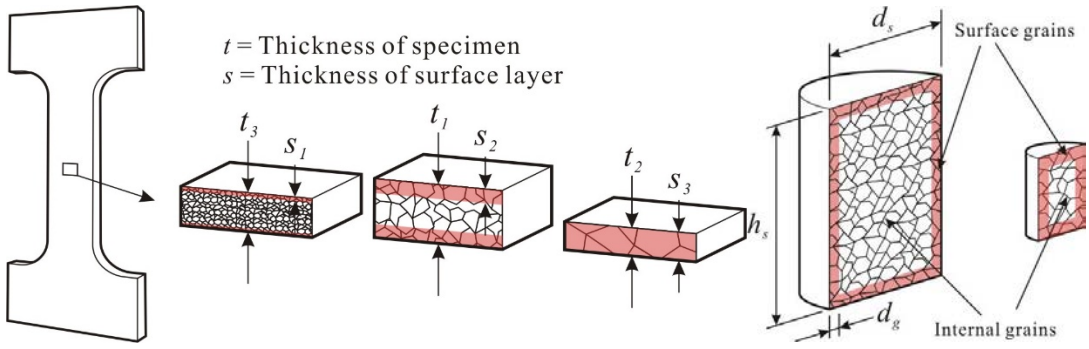

Fig. 20. Variation of the fraction of surface grains with the geometrical and grain sizes of samples [57, 64].

In the surface layer model, the mechanical properties of outer surface grains are thought to be similar to single crystal, while the interior grains are taken to have the properties of a polycrystal

[89]. The basic crystal plasticity theory expressed in the form of Schmid law [56] specifies that the single crystal flow stress can be expressed as:

$$\sigma_s(\varepsilon) = m\ \tau_R(\varepsilon), \tag{12}$$

where m is the orientation factor for slip. In addition, the Hall–Petch relation is the most widely accepted empirical theory relating yield stress to grain size in polycrystals. This was further extended by Armstrong [90] to include the flow stress as follows:

$$\sigma_i(\varepsilon) = M\tau_R(\varepsilon) + \frac{k(\varepsilon)}{\sqrt{d}} \tag{13}$$

where $\tau_s(\varepsilon)$ is the principal shear stress, d is grain size, and $k(\varepsilon)$ is the locally intensified stress needed to propagate general yield stress across the polycrystal grain boundaries.

Building on Eqs. (12) and (13), Peng et al. [91] proposed a unified-size dependent constitutive model expressed below:

$$\sigma(\varepsilon) = \eta m\tau_R(\varepsilon) + (1-\eta)\left(M\tau_R(\varepsilon) + \frac{k(\varepsilon)}{\sqrt{d}}\right) \tag{14}$$

where m and M are the orientation factors of the surface layer and interior grains, respectively. To study the SE, this model is represented by two distinct terms: the size dependent and independent parts. The material deformation model can thus be formulated as:

$$\begin{cases} \sigma(\varepsilon) = \sigma_{ind} + \sigma_{dep} \\ \sigma_{ind} = M\tau_R(\varepsilon) + \dfrac{k(\varepsilon)}{\sqrt{d}} \\ \sigma_{dep} = \eta\left(m\tau_R(\varepsilon) - M\tau_R(\varepsilon) - \dfrac{k(\varepsilon)}{\sqrt{d}}\right) \end{cases} \tag{15}$$

Fig. 21 illustrates that the above description captures the transition from single crystal to polycrystalline behavior when the volume fraction η does not exceed unity. For both the size

dependent and independent parts, the stress decreases with the increase of surface grain volume fraction. When the value of η approaches unity, the single crystal deformation scenario is realized, and the flow stress is equal to twice the shear stress, which is consistent with the experimental observations on m-scale single crystal samples. The simulated results based on this model match the experimental results well and shown in Fig. 21.

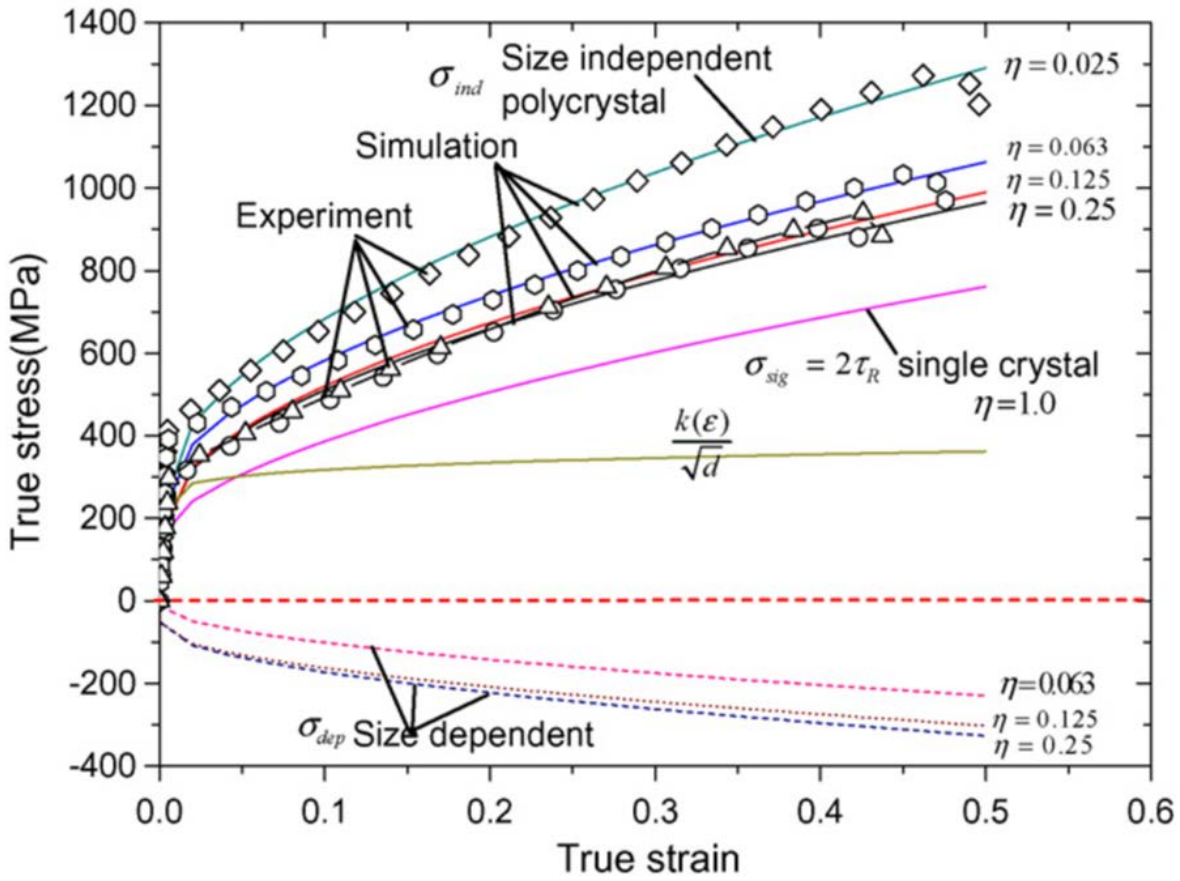

Fig. 21. Comparison of the experimental results and the prediction by Peng's model [91].

4.2. Composite model

The composite model was proposed by Meyers [40] who considered polycrystalline metallic alloy as a composite material consisting of a continuous network of work-hardened grain boundaries and discontinuous inner grains. This model has been proven to be an effective approach for establishing the relationship between material yield stress and grain size [92, 93]. The flow stress of polycrystalline aggregate is expressed as

$$\sigma_p = f_{GI}\sigma_{GI} + f_{GB}\sigma_{GB} \tag{16}$$

where σ_p is the flow stress of polycrystalline aggregate, σ_{GI} and σ_{GB} are the flow stresses of grain interior and grain boundary phases. f_{GI} and f_{GB} are the volume fractions of grain interior and grain boundary materials. The latter can be represented by grain size d and grain boundary layer thickness t_g. In general, grain boundary thickness t_g is related to grain size, which can be articulated by the following empirical equation [94]:

$$t_g = kd^n (0 < n < 1) \tag{17}$$

where k and n are constant for a given material.

Combining Eqs. (16) and (17), the following relationship is established:

$$\sigma_p = \sigma_{GI} + \frac{16}{3^{-0.5}} k\left(\sigma_{GS} - \sigma_{GI}\right) d^{n-1} \tag{18}$$

When n=0.5, Eq. (18) reproduces the Hall-Petch relationship.

In addition, Liu et al. [41] combined the composite model of polycrystal with the surface layer model used to explain the geometry SE on flow stress, and proposed a new constitutive model illustrated in Fig. 22. Based on this approach, the detailed constitutive models were developed for bulk specimens with round cross-section and sheet metals with rectangular cross-section. The flow stress of materials was designated as the weighted average of the stresses in the interior and the surface layer of specimens given by Eq.11.

The expression for the overall flow stress is derived based on the assumptions that (i) the flow stress of interior grains equals that of polycrystalline aggregate, $\sigma_i\left(\varepsilon\right) = \sigma_p$, and (ii) that the grains in the surface layer do not have the grain boundary strengthening effect and their flow stress is equal to that of the grain interior, i.e. $\sigma_s\left(\varepsilon\right) = \sigma_{GI}$. Therefore, the overall flow stress is given by:

$$\sigma(\varepsilon)=\sigma_{GI}+\frac{16}{3^{-0.5}}\eta k\left(\sigma_{GB}-\sigma_{GI}\right)d^{n-1} \tag{19}$$

The predictions of this model were verified by the comparison of FEM simulation and experimental results in μ-scale upsetting and extrusion of bulk metals and μ-tensile tests of sheet metals with different scaling parameters. Good agreement between simulation and experiment shows the efficiency of the developed model and its capability in prediction of the SE on deformation behavior in μ-forming process.

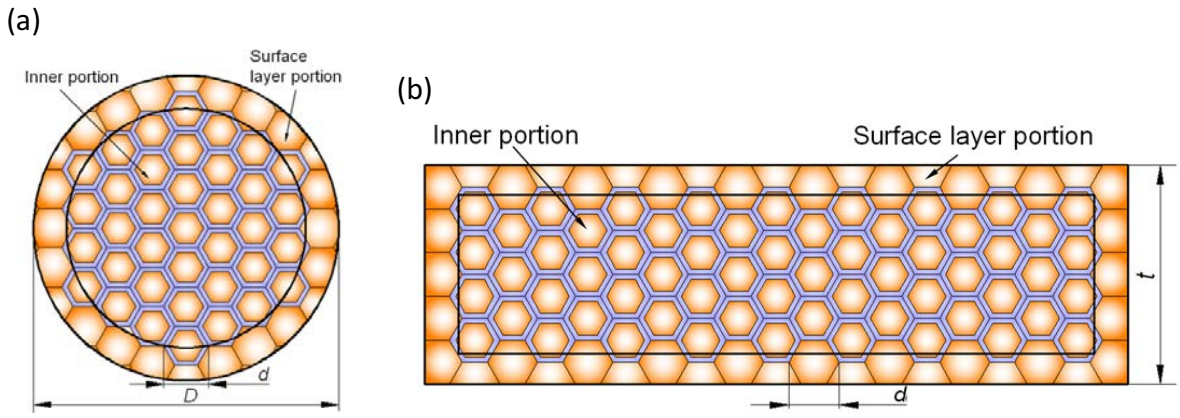

Fig. 22. Schematic of the surface layers and interior regions in (a) bulk and (b) sheet samples [41].

4.3. Crystal plasticity modeling

Crystal plasticity theory [95] allows the average shear stress concentration at the tip of a slip band to be expressed in terms of the lattice friction stress and dislocation interaction. To describe the strengthening effect due to dislocation interaction and in relation to the grain size, Ashby [55] proposed a model that introduces two kinds of dislocations referred to GND and statistically stored dislocations (SSD). The SSDs are responsible for accommodating uniform plastic strain and do not contribute to the SE, while GNDs are associated with plastic strain gradient and lead to the emergence of an additional length scale [19]. In a series of experiments, the strain gradient length scales for six different materials (Al, Ag, Ni, Cu, α-TiAl and γ-TiAl) were found to be 2.8 μm, 6.2μm, 4.3 μm, 1.1 μm, 74 nm and 49 nm, respectively [96]. In a different study, the length scales

of 12 μm and 5.8 μm were found for annealed and cold worked copper, respectively [97]. Michel and Picart [98] simulated the material behavior taking into account the strain gradient plasticity SE for sheet metal forming of very thin components. Furthermore, Ran and Fu [99] proposed a hybrid model which combines crystal plasticity theory and surface layer modelling to predict fracture strain in the alloys composed of either a single phase or multiple phases. Based on crystal plasticity theory, SEs were modeled by Zhuang et al. [72, 100, 101].

The key conclusion that can be drawn from strain gradient crystal plasticity modeling is that intricate connections exist between sample size and shape and deformation condition, on the one hand, and non-uniformity of plastic deformation at the grain level, including the associated strain gradient effects, which are a non-trivial issue to be explored and systematically studied in a great extent.

4.4. Lubricant pocket model

The influence of SEs on frictional behavior in μ-scale deformation processes was investigated using scaled ring compression tests and double cup extrusion (DCE). It was found that the so-called open and closed lubricant pockets, as shown in Fig.23, are responsible for the SE [12]. Punch contact with workpiece causes asperity flattening that defines the real contact area (RCA).Since the initial workpiece surface is not perfectly smooth, some lubricant is trapped in roughness valleys called closed lubricant pockets (CLPs). When lubricant can escape from some roughness valleys, these are referred to as open lubricant pockets (OLPs).

Before the punch contacts the material surface, a continuous layer of lubricant is present at the surfaces of workpiece (Fig.23a). When the punch establishes contact with material surfaces, some lubricant is contained in CLPs. Upon further approach of surfaces under external load, oil can be squeezed out from the OLPs, as shown in Fig.23b. However, some oil is trapped in roughness valleys, resulting in the formation of CLPs. The increasing hydrostatic pressure generated in CLPs provides additional contact support that promotes low friction sliding along the

tooling surface. In contrast, when lubricant is squeezed out of the OLPs, the related asperities are flattened, becoming RCAs. In the course of deformation process, the RCAs increase with further compression, resulting in the increase of interfacial friction, as shown in Fig.23c.

This model can be applied to the analysis of the DCE test with a scaling effect related to

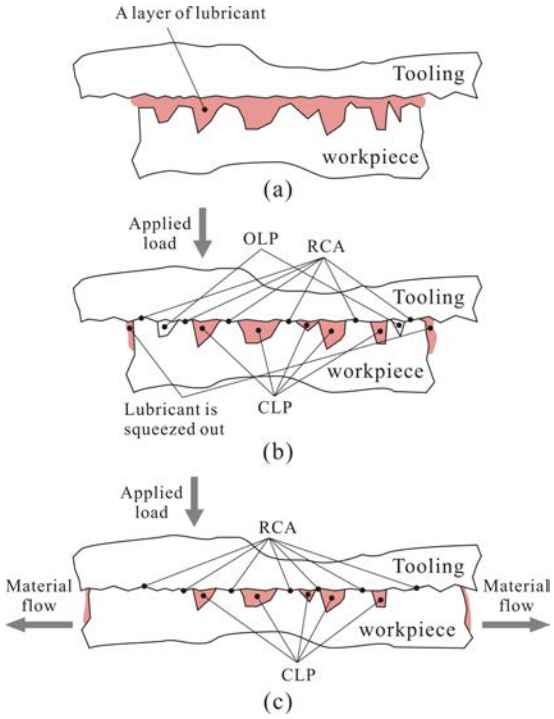

Fig. 23. Graphical illustration of the evolution of surface topography in contacts [102].

the ratio of open to closed lubricant pockets. There is a region of constant width (w) where the open lubricant pockets become effective, as shown in Fig.24. This means that the size of the OLP region does not change with the specimen size. The contact region can be identified via roughness measurement at the outer surface of the extruded samples that shows distinct flattening of asperities illustrated in Fig.25. However, Deng et al. [102] stated that the change of OLP margin width is not proportional to sample size, as seen in experiments on compression of differently sized copper cylinders. The main reason of the increase of friction with sample miniaturization is actually the increase in the OLP fraction. Furthermore, the effect of asperity size on sample surface topography after compression testing is illustrated in Fig. 26. The width of the OLP margin is seen

to decrease with increasing asperity size. This indicates that the efficiency of lubricant is significantly higher in the case of large asperities, which may be tentatively explained by the fact that large asperity valleys contain more lubricant, leading to the increase of the area fraction of CLPs. The model of OLPs and CLPs and its effect in scaling has been confirmed by additional independent investigations [32, 103, 104].

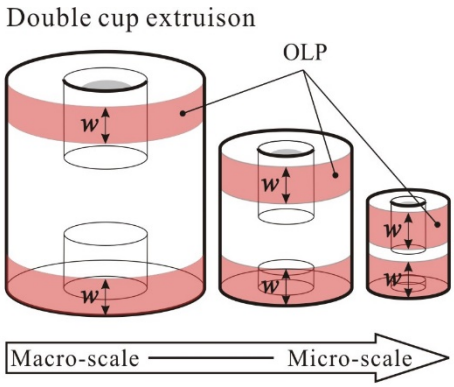

Fig. 24. The width of OLP does not change with the scaling down of workpiece size (*w* is the width of OLP) [13].

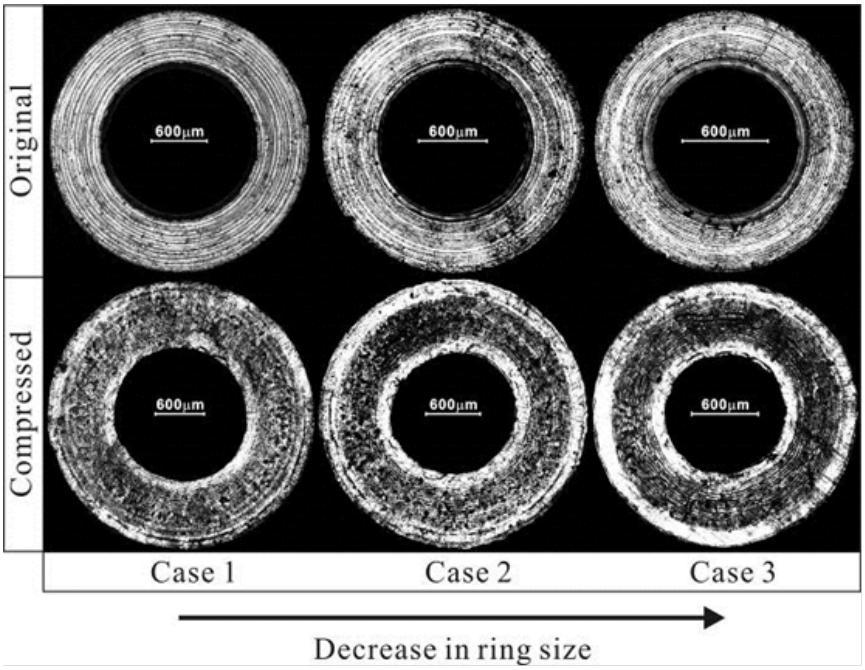

Fig. 25. SEM photographs of the end surfaces of ring samples before and after compression. Original specimen dimensions: Case 1 Ø3×Ø1.5× 1mm; Case 2 Ø2.5×Ø1.25×0.83mm; and Case

3 Ø2×Ø1×0.67mm [57].

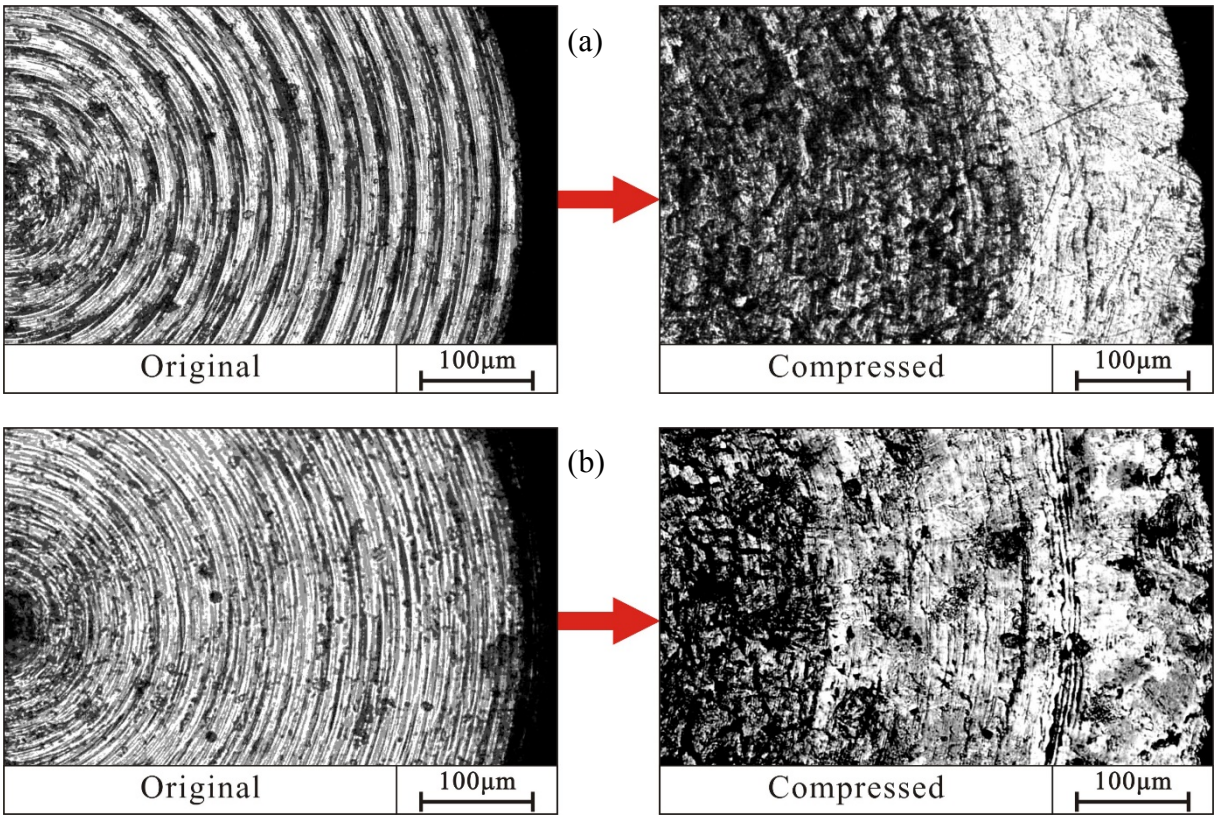

Fig. 26. End surface images of compressed test samples (Ø1×1.5 mm) with asperity size of (a) 25μm, and (b) 10μm [102].

In modeling of the SE mechanisms, different models have been proposed, which are basically phenomenological and are able to explain the corresponding phenomena. In compression and tension based deformation where SSDs play a big role to accommodate uniform plastic deformation, the flow stress is decreased with the geometry size of workpiece, which can be well explained by the surface layer model as the percentage of surface grains is great and they dominate in the deformation process. However, in microbending process where GNDs are more responsible for nonuniform deformation, viz., the existence of plastic strain gradient, the surface layer model fails to explain the SE well. Taking the microbending shown in Fig.7 as an instance, when the foil thickness t_o is larger than 100 μm, the springback angle is reduced with the foil thickness. There exists a phenomenon that the smaller springback angle, the lower flow stress and the smaller foil thickness. This is the so-called "the smaller, the weaker", which is in tandem with the essence of the surface layer model. When the foil thickness t_o is reduced to smaller than 100 μm, the

springback angle, however, increases (indicating the increase of flow stress) with the decrease of foil thickness t_o , showing the phenomenon of "the smaller, the stronger", which cannot be explained by the surface layer model, but may be amenable to the treatment using strain gradient plasticity theory. Therefore, phenomenologically based models have their limitations and there is still significant room to explore in terms of modeling and study of the SE mechanisms.

5. μ-forming performance aspects related to SEs

5.1. Uncertainty and scatter due to SEs

Two measures of processing performance can be defined, the required deformation load and the dimension accuracy of μ-formed parts. Large scatter observed in these two performance indicators is a critical issue for product quality assurance and control in mass production of μ-scale parts by μ-manufacturing, since for the same material, tooling setup and deformation conditions used in production, key performance indicators such as dimensional accuracy can vary by 15% to 20 %. Understanding the origins of this scatter and the means of controlling and reducing it are relevant to the topic of the present review.

5.1.1. Scatter of the deformation load

As a general rule, deformation uncertainties increase with sample miniaturization by proportional scaling. With the decreasing specimen size, the overall flow stress tends to decrease, leading to lower load required for deformation, and increasing the effects associated with stochastic influences that may be present at sample free surfaces, e.g. air bending [30, 60, 105]. Grain SEs become more prominent with smaller dimensions [19]. However, it has also been observed that forming forces increase again with miniaturization beyond certain size. This phenomenon is likely to be associated with the situation when approximately one grain spans the

entire thickness of a sheet. In this regime, the processing force tends to increase with increasing grain size, as shown in Fig. 27. This deviation from the Hall-Petch relation [106, 107], that is often used as received wisdom in the context of metal forming at conventional dimensions, is clearly associated with the change in deformation mechanism: whereas for polycrystalline materials, the strain can be assumed to be somewhat homogeneous overall (although local variations are present, as discussed above). In μ-scale deformation with the reduced number of grains, deformation imposed by the tool shape is accommodated differently depending on the grain orientation and the availability of slip systems [14]. This means that if grain orientation within the workpiece is not controlled and is unknown, then the deformation load displays a significant amount of scatter. This situation is similar to that encountered in the experimental analysis of stresses at the μ-scale using Focused Ion Beam and Digital Image Correlation (FIB-DIC) ring-core milling that calls for uncertainty quantification due to unknown underlying crystal orientation [108].

The scatter of deformation load in compound μ-scale deformation processing is also apparent. Fu et al. [109] conducted μ-blanking and deep drawing compound processing using copper sheet with different feature and grain sizes to study the deformation behavior in the process. It was found that the forming load decreased with the increase of grain size, but this decrease is not significant when only a few grains were found in the cross section of the sheet metal, as illustrated in Fig. 28. The deformation became inhomogeneous with the decrease of the formed part size and the increase of the grain size. This leads not only to irregular final geometry and rough surface finish of the formed part, but to a greater amount of scatter of the forming parameters, including the overall deformation force required.

In contrast with the deformation load behavior for specimens with free surfaces, no significant decrease in forming force is observed in the case of closed die forming processes, such as extrusion. In fact, the forming forces typically show an increase that could be explained by the increase in friction. In μ-deformation process involving closed dies at room temperature, the decrease in the part dimensions results in an increase in the effective overall stress expressed as the punch force

divided by its cross-section area [14]. When the effect of grain size on the processing force and strain distribution within μ-blanking and bending tests was investigated, it was found that it is quite difficult to develop a universally applicable FEM model, despite a significant amount of work devoted to addressing this issue [19]. This suggests that the scatter in the results arises from a lack of appropriate model formulation taking into account all aspects of the process that affect the outcome from modeling and simulation perspectives.

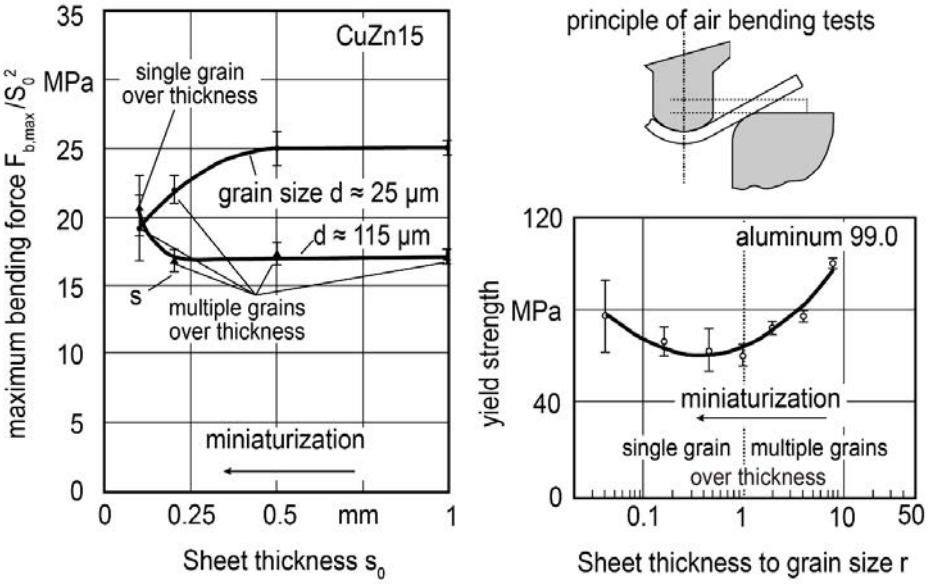

Fig. 27. Normalized bending forces and overall yield strength in bending deformation process showing the effect of geometrical and grain sizes [11].

In general, therefore, as the sample dimensions are decreased, the scatter in the forming force tends to become greater. Chan and Fu [35] found a significant scatter of the measured deformation pressure in μ-heading processes, as illustrated in Fig 29. For the coarse-grained material, the scatter can be explained by the individual grain properties becoming dominant in the overall deformation behavior when the ratio of specimen size to grain size decreases. In a backward extrusion operation, the scatter in the forming force grows with the transition from ultrafine-grained copper to coarse-grained material [110]. It was also observed that increasing scatter of grain size also increased the scatter of forming force [19].

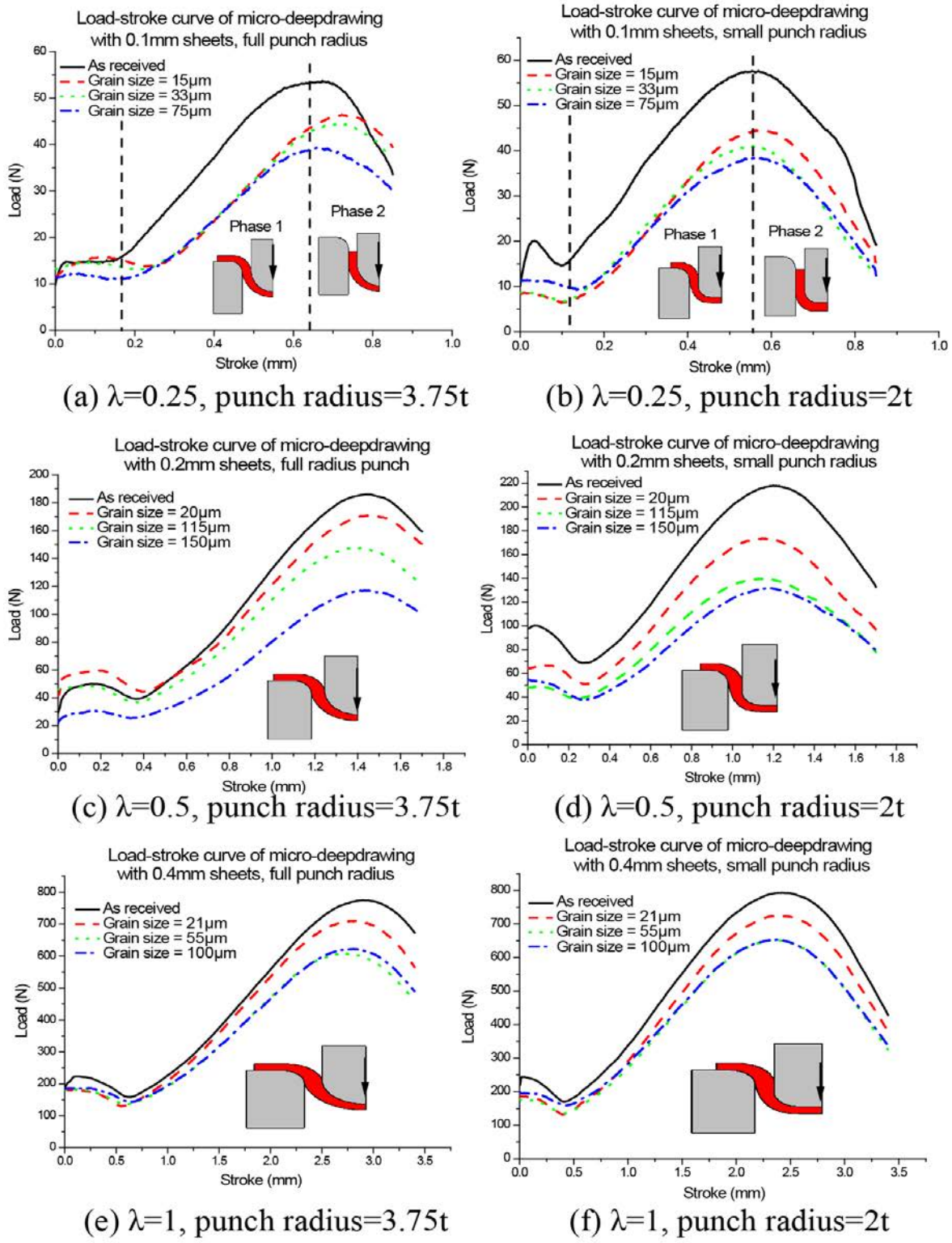

Fig. 28. Load–stroke curves in μ-scale deep drawing processes. Scaling factor λ=1 refers to the sheet thickness t = 0.4mm, dia. of drawing die is 4.2 mm, dia. of drawing punch is 3mm, dia. of blanking punch is 6.6mm, radius of drawing die is 0.8mm, and clearance is 0.6mm. Other values of λ correspond to scaling down these dimensions [109].

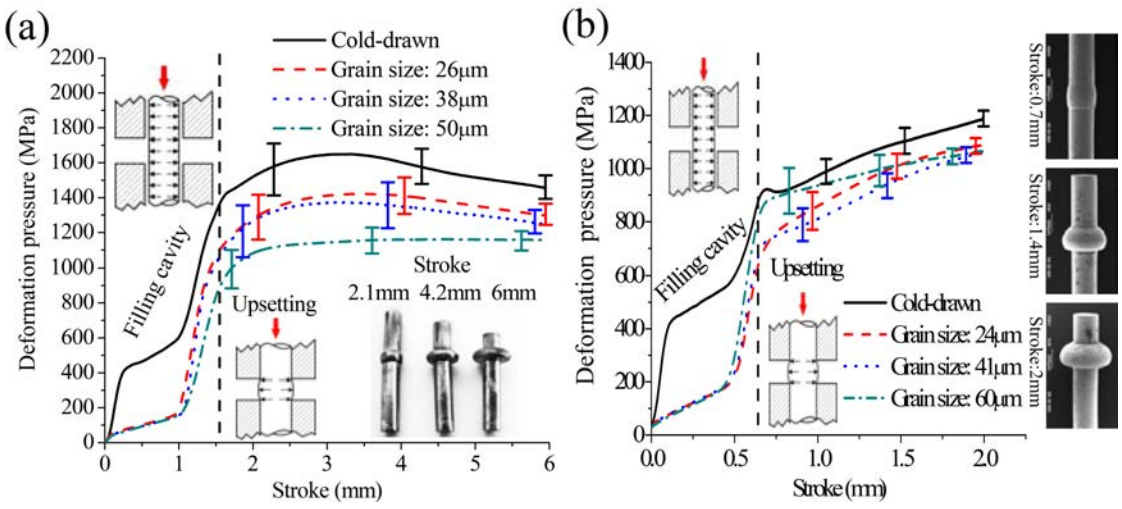

Fig. 29. The deformation pressure *vs* stroke plots during heading operation at the (a) macro- and (b) μ-scale [35].

5.1.2. Scatter in the shape accuracy

To achieve net-shape or near net-shape forming in μ-scale deformation processes, shape accuracy represents an important quality parameter. Krishnan et al. [111] conducted μ-extrusion using CuZn30 brass workpieces to produce pins with a circular cross section that have a final extruded diameter ranging from 1.33 down to 0.57 mm. Fig. 30 illustrates the shape of the extruded samples. Using a single extrusion die with reduction in diameter from 0.76 to 0.57 mm, using starting stock material with the grain size of 32μm to produce straight pins, whilst using the stock with the larger grain size of 211μm led to 60% of the pins produced having large uncontrolled curvature. The occurrence of curved samples can be attributed to the effect of inhomogeneous deformation in the coarse-grained samples containing a small number (about four) grains across the diameter of the initial workpiece. In contrast, fine-grained samples contained on average more than 20 grains across the diameter, leading to good property averaging and uniformity of deformation, so that no significant curvature is observed even after multiple repeated extrusion processing. These results show that the size, orientation, and distribution of grains play an important part in extrusion. Furthermore, the μ-scale backward extrusion carried out using a partly transparent tool revealed the importance of local flow behavior of individual grains for the overall shape accuracy: the

homogeneity of material flow decreased with the decreasing ratio of the extruded wall thickness to grain size [19].

In order to investigate the micromechanical damage and deformation behavior in progressive μ-scale deformation processing, Meng et al. [112] fabricated a μ-cylindrical part by shearing deformation and a multi-level flanged part via progressive μ-extrusion and blanking, as illustrated in Fig. 31. It is apparent from Fig. 32 that the undesirable deviation of the deformed shape occurs with the increase of grain size, leading to a significant shape scatter. Significant variation in the inclination of the flanged feature, irregular shape and the presence of an obvious burr were found in the workpieces using coarse-grained material. This is another manifestation of the SE and orientation of individual grains affecting significantly the material flow behavior when the characteristic dimension of the sample reaches the order of magnitude of grain size.

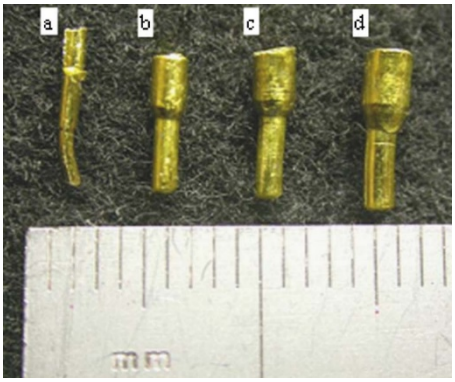

Fig. 30. Four deformed pins produced by extrusion using the dies with different dimensions: (a) 0.76: 0.57, (b) 1.50: 1.00, (c) 1.75: 1.17, and (d). 2.00: 1.33 mm [111].

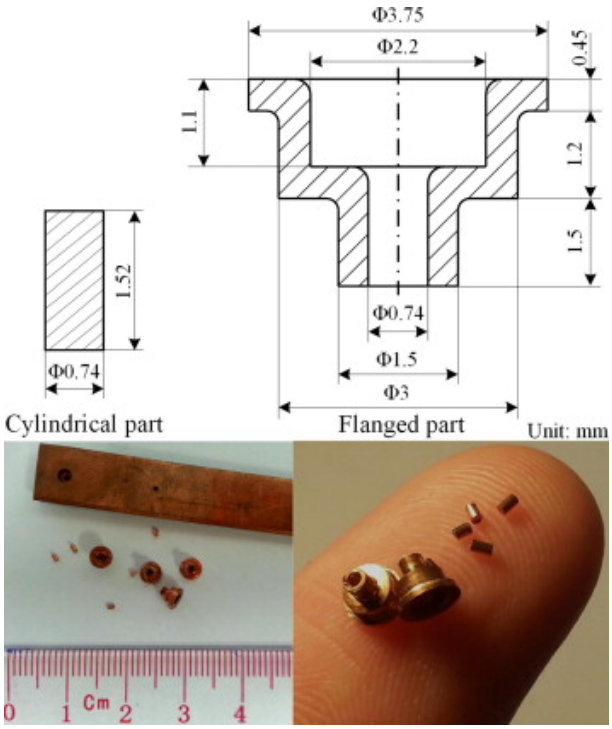

Fig. 31. Progressively μ-formed cylinders and flanged parts [112].

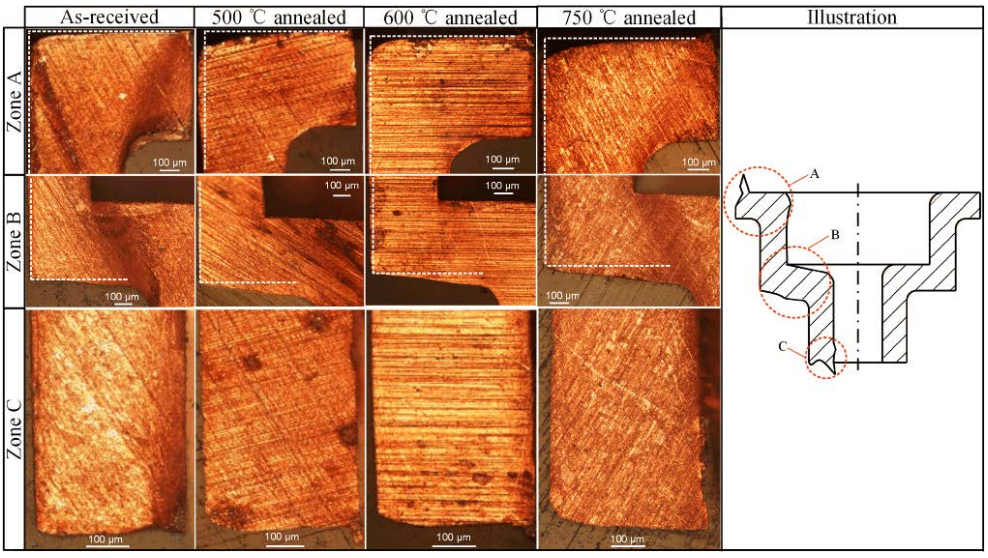

Fig. 32. Geometrical features of the flanged part produced by progressive forming [112].

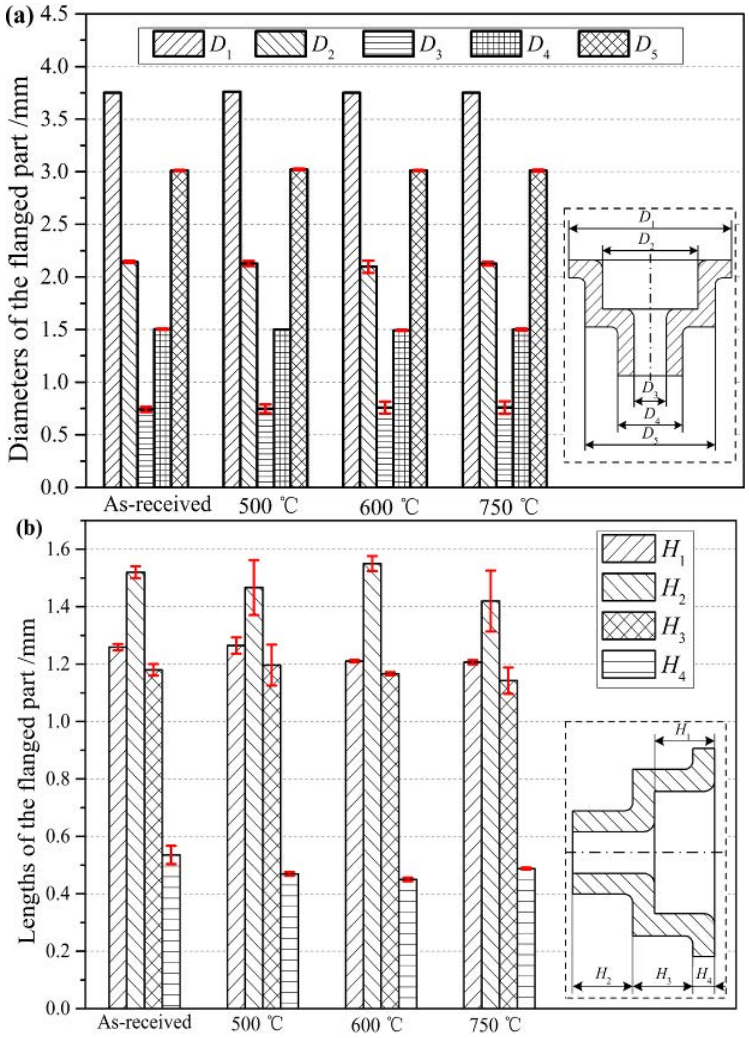

Fig. 33. Dimensional scatter in a flanged part: (a) diameter, and (b) length [112].

In order to evaluate the grain SE on the dimensional accuracy quality of the final part, three two-level flanged parts were formed and measured for different billet materials, as illustrated in Fig. 33 [112]. It was found that the diameters of the flanged part were consistent for both fine-grained and coarse-grained materials, due to the fact that the deformation along the diametrical direction was restricted and strictly controlled by the diameters of tooling. In contrast, free deformation occurred in the length-wise direction. The variations or scatter of H_2 and H_3 height parameters present a decreasing trend with the decrease of the grain size. Height H_4 representing the thickness of the flanged feature after extrusion was reported to show a rising tendency with the decrease of grain size. Significant scatter in the results was observed in the annealed condition

that can be attributed to the growth of grains and thus leading to deformation irregularity and inhomogeneity, and further causing the unrepeatable deformation. Compared with the fine-grained material, the standard deviation of geometric dimension was increased in the case of coarse-grained material, indicating that the shape stability of the formed part worsens with the increase of grain size due to deformation inhomogeneity.

Springback behavior is a major concern in μ-scale sheet metal forming. The reason for this is the inevitable springback which affects the dimensional accuracy of the final part. Taking bending as instance, there are generally two different SEs identified. The first SE caused by material microstructure: when the workpiece dimensions are scaled down, the ratio of surface grains to the overall volume increases, leading to a decrease in the overall apparent material resistance. The second SE is induced by the large strain gradient appearing when the foil thickness is decreased, which results in an increase in the overall material strength. Diehl et al. [113, 114] conducted experimental and numerical investigations and stated that the first effect (a decrease in spring-back angle) is dominant when the scaling factor is greater than 0.2, whilst for lower scaling factor, the second effect is dominant (an increase in springback angle), as illustrated in Fig. 34. Gau et al. [29] investigated the springback behavior of brass by three-point bending. It was found that the smaller t/d ratio, the lower springback observed.

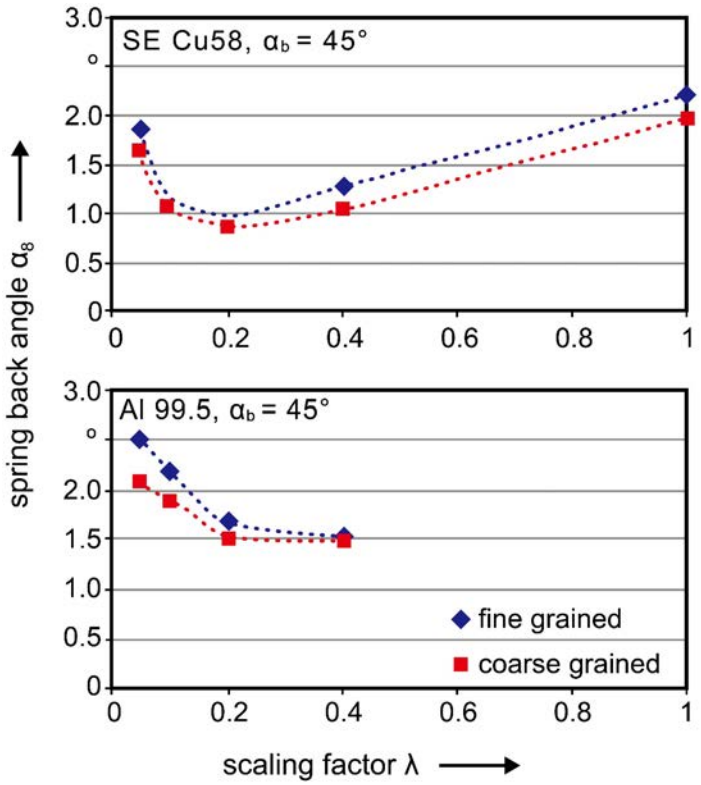

Fig. 34. Influence of scaling factor λ on springback angle (λ=1 corresponds to the punch radius of 500μm, clearance between punch and bottom die of 240μm, and punch velocity of 4mm/min) [113].

5.1.3. Scatter of dimensional accuracy

Meng et al. [115] extensively studied the material deformation and fracture behavior in shearing process to pre-pierce a hole or to blank a cylindrical part, as shown in Fig. 35. It is revealed that they have a significant effect on the subsequent operations and the quality of the fabricated parts. The interactive effects of multiple factors including grain size, lubrication condition and shear velocity on the quality of both the blanked part and the pierced hole were investigated. It was found that the forming quality became worse with the increase of grain size and shear velocity. Fig. 36 shows the change of the cylinder height h and diameter d_b with the average grain size using different lubricants. It was found that the length of the cylindrical part decreased with grain size, while the part diameter reached a maximum value and then decreased. Chan and Fu [116] found that the length of the blanked cylinder decreased with the grain size,

which was attributed to a large amount of lateral material flow taking place in the coarse-grained material.

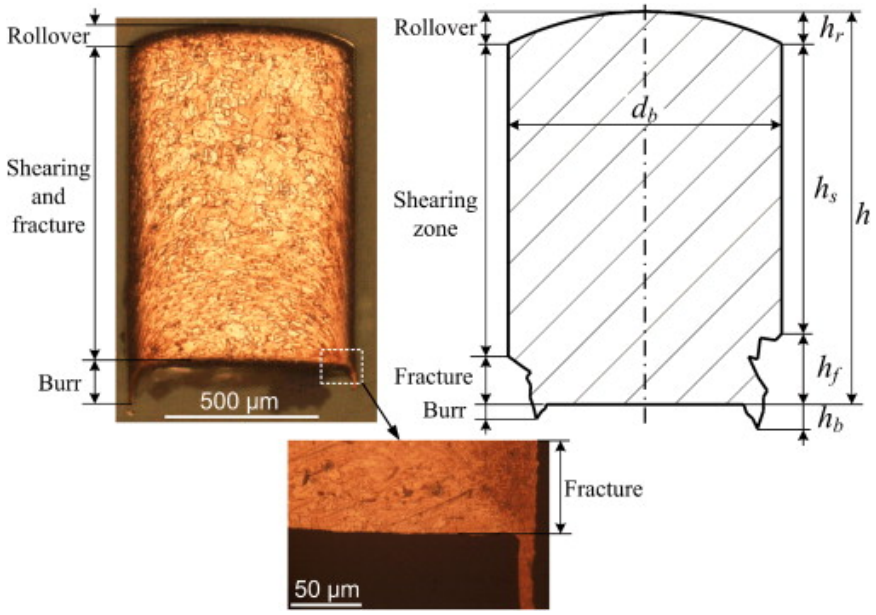

Fig. 35. Different deformation zones in a sheared μ-part [115].

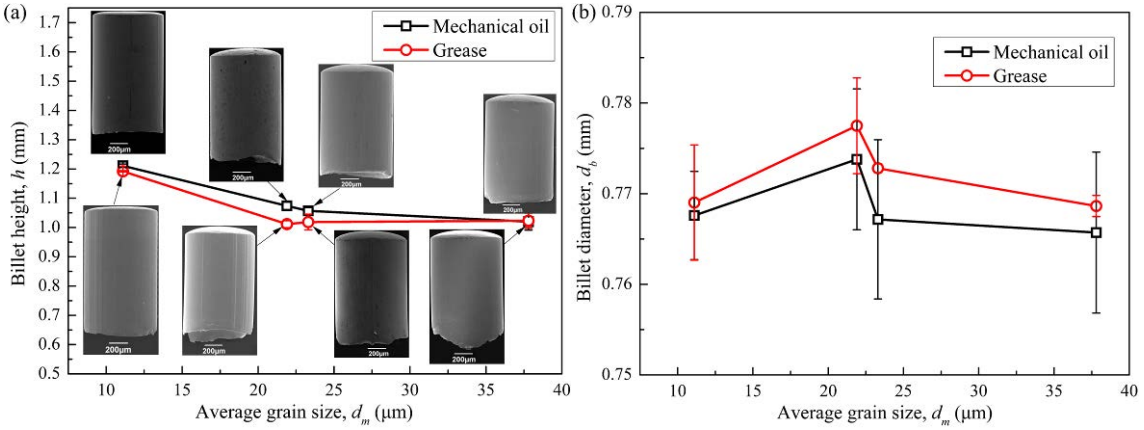

Fig. 36. Dimensional variation of the blanked cylinders: (a) height and (b) diameter [115].

In order to further investigate the dimensional variation of the blanked cylindrical μ-part, the volume of the blanked part was calculated from the measured dimensions, as shown in Fig. 37. It can be seen that the part volume reduced with the grain size due to a small amount of deformation in shear band in the coarse-grained material. The frictional resistance of the lubricant grease was much smaller than that of mechanical oil, bringing about a large amount of deformation in the

lateral direction. Therefore, both the sheared part length and the volume were reduced due to the use of grease lubricant.

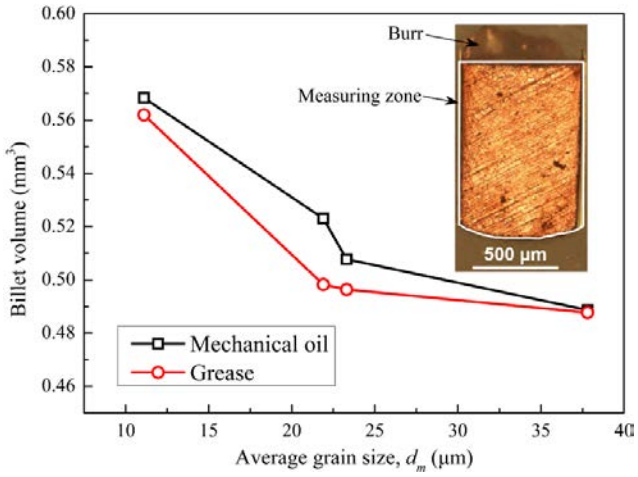

Fig. 37. Change of the blanked cylinder volume versus grain size [115].

The blanked cylinder can be divided into four deformation zones that can be identified as rollover, shearing, fracture and burr, as shown in Fig.35. The depth percentage of these regions is shown in Fig. 38. It can be seen that both the rollover and burr zone sizes increase with grain size, while the shearing and fracture zones decrease with grain size. The length of the burr is closely related to the interaction between grain size and punch-die clearance, and reaches a peak when the grain size is approximately equal to the punch-die clearance. From the figure, it is concluded that the variation of dimensions is caused by different grain sizes.

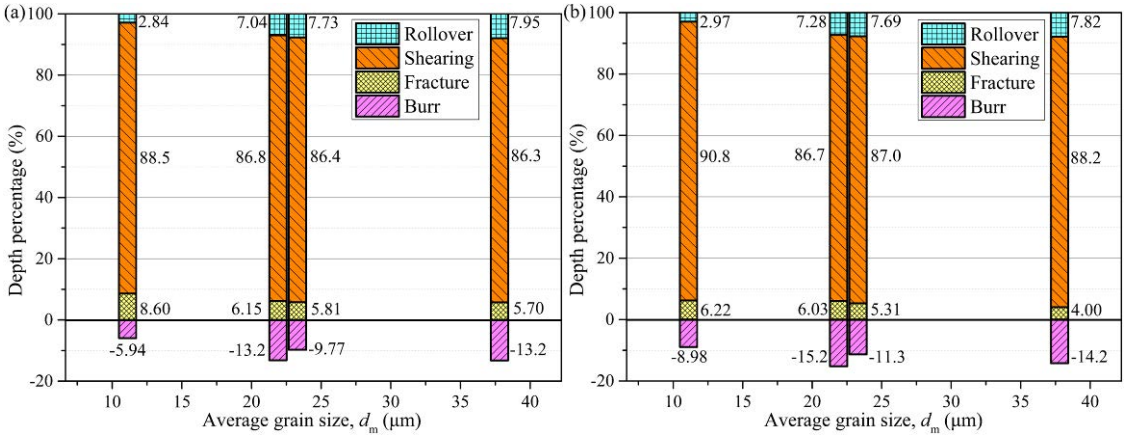

Fig. 38. Depth percentage of different features of the extruded part using (a) mechanical oil, and (b) grease lubricant [115].

5.1.4. Scatter of flow pattern and flow-induced defects

In μ-scale deformation, the anisotropy and orientation of individual grains lead to the inhomogeneity of local material flow and the scatter of flow pattern, which could further induce flow defect and affect the quality of μ-formed parts. Flow-induced defects in μ-scale parts are more severe than those in m-scale due to the greater inhomogeneity of material flow in μ-scale deformation. To explore the flow-induced defects in different size-scaled deformation, Wang et al. [47] used two different geometries of scaled non-axisymmetrical parts and the materials with different grain sizes to investigate the SE on flow-induced defects, viz., folding defects, as shown in Fig. 39. The geometry SE had a greater influence on the formation of folding defects than microstructural or grain SE. With the decrease of geometrical dimensions of μ-parts, the severe folding defects in the formed parts showed a remarkable reduction independent of grain size.

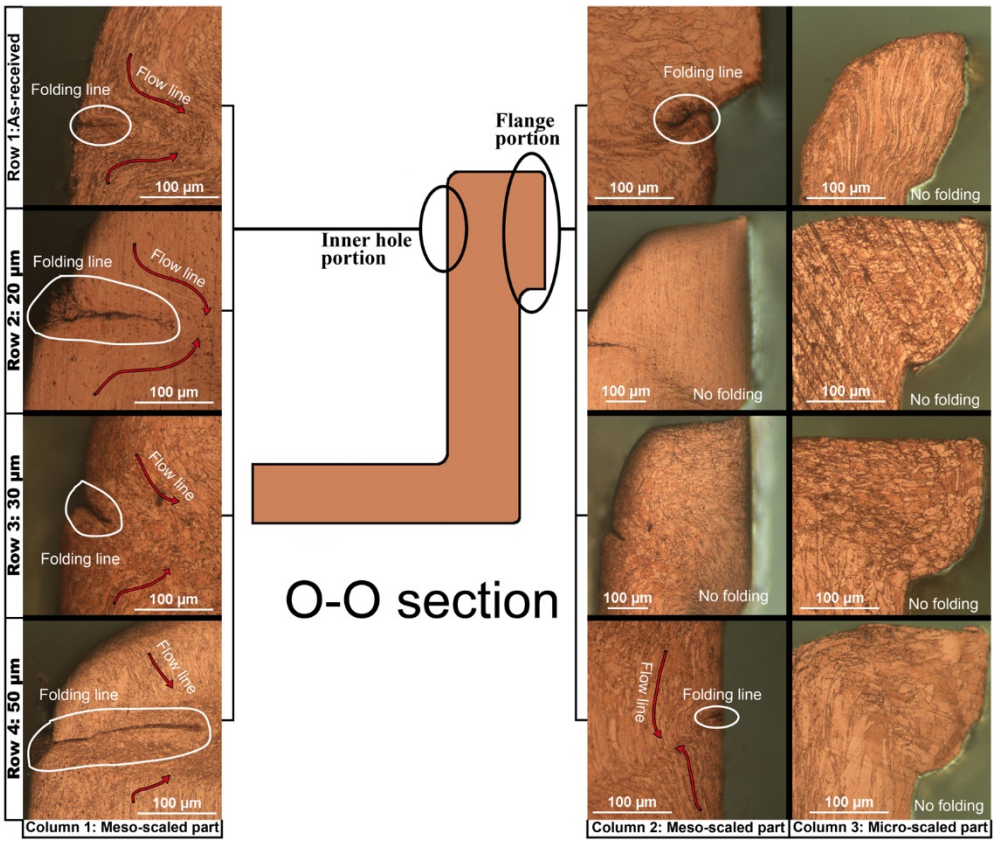

Fig. 39. Folding defect formation in the meso- and μ-scale formed parts with different grain sizes [47].

5.2. Variation and distribution of hardness

Work hardening is important for the superior mechanical properties of the deformed parts. It can be characterized by the hardness value and its distribution within the workpiece, which is actually affected by the work hardening phenomenon, and therefore closely related to the plastic strain distribution within the workpiece. Brinell hardness was measured as a function of grain size for α-brass, copper, bronze, and commercially pure Armco iron. A linear relationship was found to apply between the hardness and the inverse root $d^{-1/2}$ of grain size d, as illustrated in Fig. 40. This is in accordance with the Hall-Petch relationship [117]. Farhat et al. [118] reported similar results obtained by performing hardness measurements using an ultra-microhardness indentation system. They concluded that even within the grain size range of 15-100 nm, the hardness *vs* grain size data could be well represented by the Hall-Petch relationship.

However, when the grain size of materials exceeds 100μm, the measured hardness may not reflect the material characteristics precisely, because the indentation impression does not cover a sufficient number of grains to provide good averaging. Therefore, for the case of coarse-grained materials, the hardness values and their spatial distribution display different features compared with the case of fine-grained materials. Through the measurement of the μ-forward extrusion of a billet with the diameter of 0.5mm, it was found that the maximum hardness corresponded to the specific grains which experienced severe deformation due to their size, orientation, or position, as illustrated in Fig. 41. This phenomenon deserves further attention in assessing the quality of μ-formed parts.

To highlight the difference in the deformation behavior between the rollover and fracture zones, μ-hardness was measured in the vicinity of the two regions, producing the results illustrated in Fig. 42. Fig. 43 presents the variation of hardness as a function of the distance from the hole edge that was punched with the shear velocity of 0.01 mm/s. It was found that the hardness was affected by the shearing over a distance depending on the grain size and the lubrication condition.

When the fine-grained material was used, a subtle increase in the hardness was caused by a small amount of deformation at the rim of the pierced hole. However, the hardness increased by as much as about 44% when coarse-grained material was used. The shear-induced work hardening is associated with the interaction between dislocations and grain boundaries that act as an obstacle to disrupt the dislocation glide along a particular slip system. Dislocations cannot easily cross the grain boundaries due to the need to change the direction of slip and the slip plane, and the atomic disorder encountered at grain boundaries. In a coarse-grained material, the number of dislocations within the grain is larger, leading to more entanglement of dislocations in the pile-up. In contrast, fine-grained material contains more grain boundaries that make it difficult for the dislocations to move across the sample, resulting in a lower rate of increase of dislocation density. Therefore, the shearing process within a coarse-grained material has greater impact on work hardening compared to the fine-grained material. It can be seen from Fig. 43 (a) that the hardness under dry friction conditions shows a significantly higher value compared to the lubricated condition. This is because the material is subjected to severe deformation that further promotes work hardening. Compared with the regions close to rollover zone, work hardening is higher at the surface nearest to the die entrance due to the greater shearing deformation accumulation right up to the onset of fracture. It is also noticed that the extent of hardening becomes lower with the use of grease lubricant at the places with a fixed distance to the hole edge, demonstrating that high viscosity lubricant reduces the hardening slope.

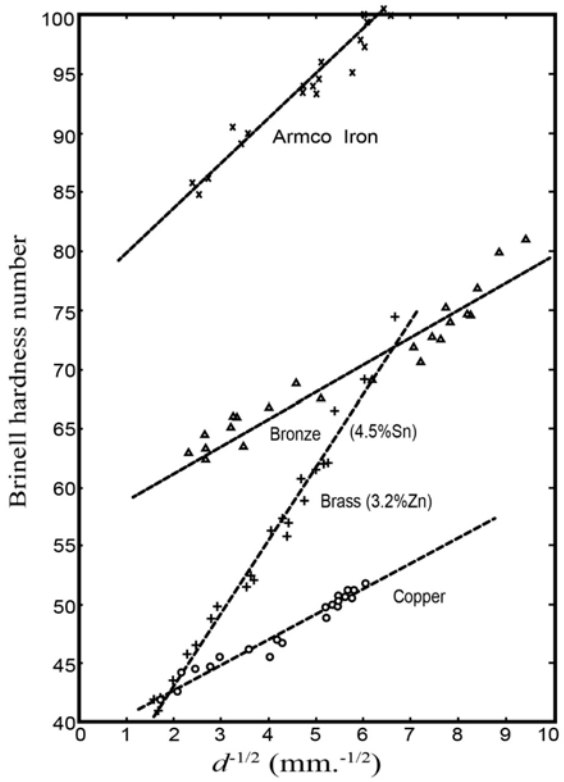

Fig. 40. The relationship between hardness and the inverse square root of grain size, $1/d^{1/2}$ [117].

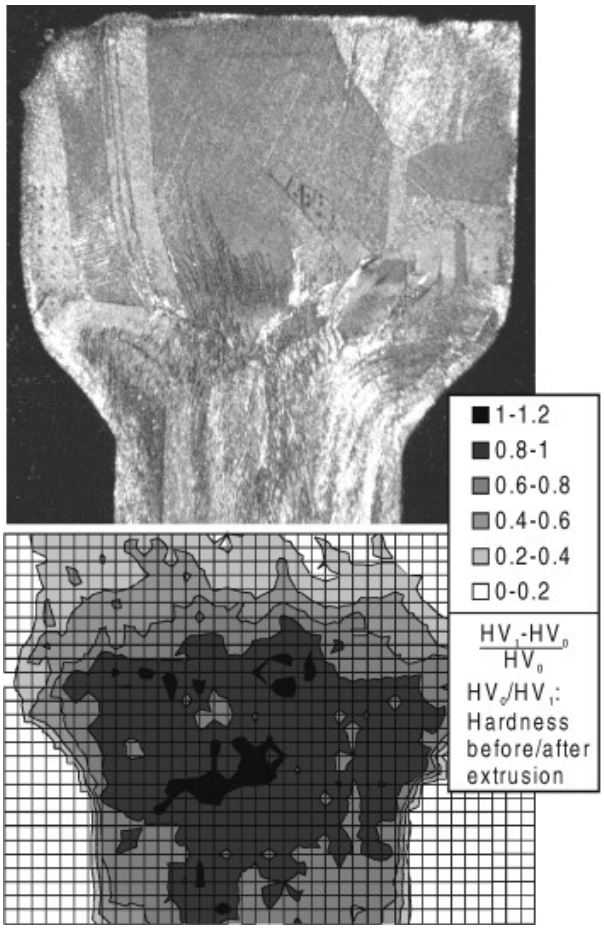

Fig. 41. Irregular hardness distribution of a coarse-grained extruded specimen [11].

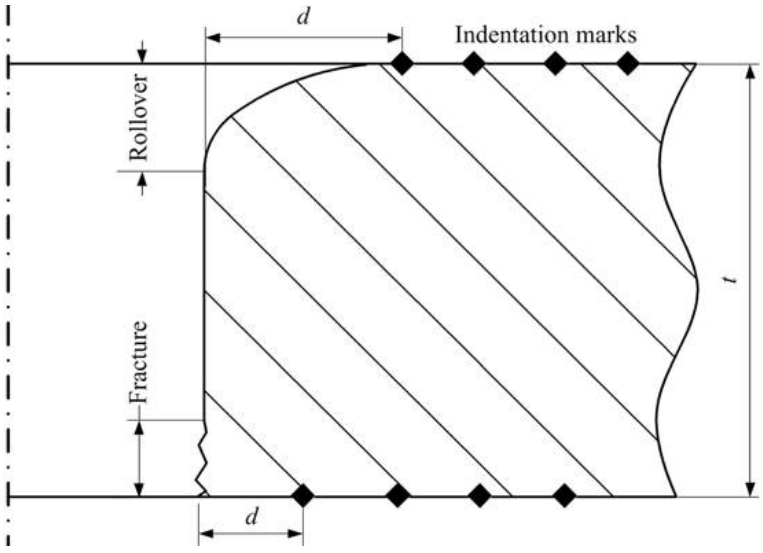

Fig. 42. The indentation positons near a pierced hole [115].

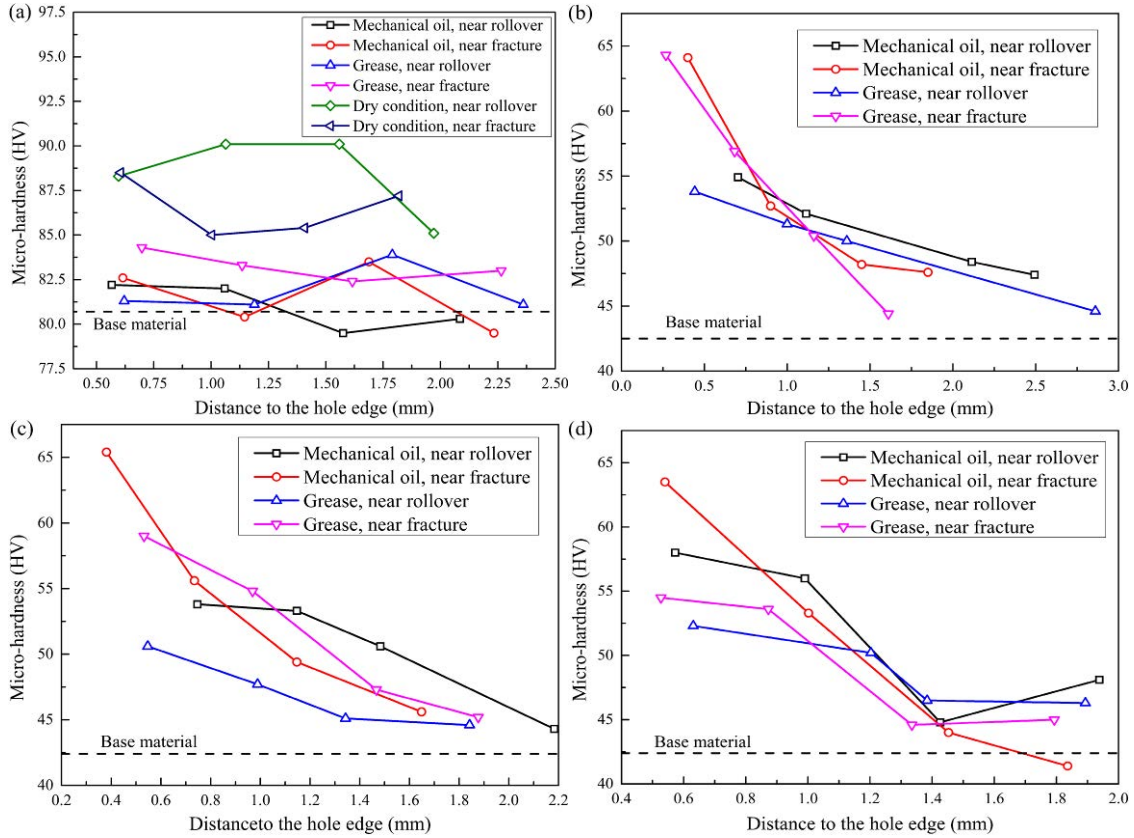

Fig. 43. Variation of μ-hardness in the vicinity of a pierced hole in the materials with grain sizes of (a) 11.1μm; (b) 21.9μm; (c) 23.3μm and (d) 37.8μm [115].

5.3. Formability

5.3.1. Sheet formability in tension

Gau et al. [119] conducted tensile tests using aluminum alloy AA1100 and brass to investigate the influence of SEs on the flow stress and formability. It was found that the yield strength and ultimate tensile strength decrease with *t/d*, the ratio of thickness to the average grain diameter, when this ratio is greater than unity. In contrast, when the *t*/*d* ratio decreases from unity, the yield strength and ultimate tensile strength increase. In addition, formability decreases with the *t*/*d* ratio. Various tensile tests were performed to investigate the SEs on the flow curves and fracture strain for pure copper [83], aluminum [120] and CuZn36 brass [121]. Experimental results show a decrease in the yield strength and maximal true strain with the decrease of grain size, as illustrated in Fig. 44.

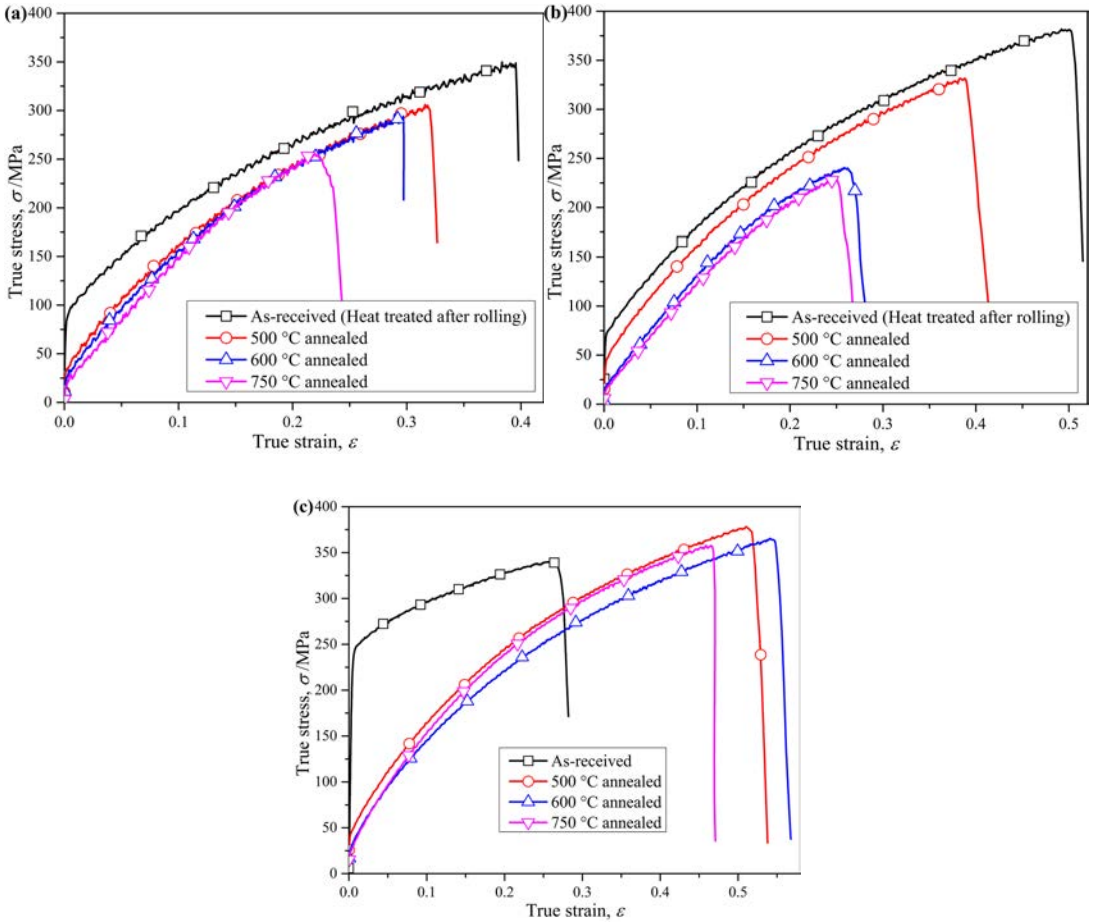

Fig. 44. Flow stress-strain relationship of pure copper sheet with thickness of t = (a) 0.2 , (b) 0.4 and (c) 0.6 mm [83].

5.3.2. Bulk formability

Ran et al. [27, 99] conducted m- and μ-scale flanged upsetting to study the SE on the fracture behavior using brass C3602. It was found that formability increases with the decrease of specimen size for a given grain size, as shown in Fig. 11. Furthermore, a hybrid model for multiphase alloys was proposed that determines the contribution of each phase to the plastic deformation behavior of material and uses fracture energy to predict the ductile fracture in μ-forming.

5.3.3. SEs on the Forming Limit Diagrams

Experimental investigations found that the forming limit represented by the strain curves appearing on the forming limit diagrams (FLD) tends to increase with sheet thickness, as shown in Fig. 45 [19]. The influence of grain size on material formability was investigated through tensile

tests and formability tests conducted using specimens with different grain size. It was found that finer grains tend to improve the formability, as demonstrated in Fig. 46. This was confirmed by a series of experiments in which the grain size was held constant and the sheet thickness was varied between 500 and 25μm. A significant decrease in the maximum strain from 0.25 to 0.05 was detected [20, 122].

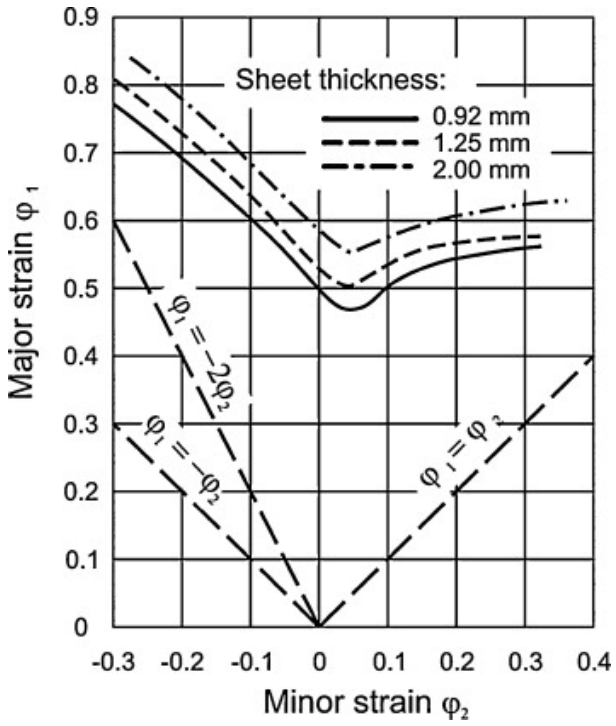

Fig. 45. Effect of sheet thickness on the FLD [19].

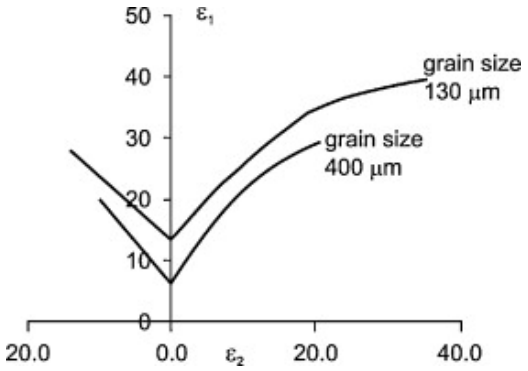

Fig. 46. FLDs of Al alloy AA1050 sheets with different grain size (t = 0.5 mm) [19].

In addition, Xu et al. [123] conducted uniaxial tensile tests using differently shaped specimens

to obtain the left hand side curve (compressive through thickness strain) in the Forming Limit Diagram for the sheet metal ranging from m- to μ-scale. Digital Image Correlation (DIC) method was also employed to measure the limit strain [124]. During the tensile test, images were captured continuously using a digital camera. Displacement and strain fields were then determined by analysis of the evolution of the captured image series. The left hand side FLD for different *t*/*d* ratios was constructed. The experimental results showed that the forming limit decreases with the *t*/*d* ratio. However, it is important to note that the scatter of the forming limit becomes much worse when a small number of grains (one or two) span over the sheet thickness. Furthermore, Xu et al. [125] obtained the full forming limit diagram for sheet metal through experiments aimed to study the SE on the formability of sheet metal in μ- and meso-scale plastic deformation. Samples were designed to obtain different deformation paths from uniaxial to biaxial stretching conditions, as shown in Fig. 47. The results are presented in Fig. 48. The conclusions about the thickness of 0.4 mm are similar, in which the FLD was shifted down with the decreasing ratio of the thickness to grain size, *t/d*. For the case with the thickness of 0.2mm shown in Fig.48(b), the FLD shows the same trend with the grain size changing from 17.4 to 35.2 μm. When the grain size is 166.3 μm, however, FLD shows high level of uncertainty. In addition, for the case of thickness of 0.1 mm shown in Fig.48(c) the thickness and grain size are similar, leading to the experimental results becoming scattered, so that a systematic trend cannot be identified. In other words, large uncertainty persists in terms of the relationship between grain size and FLD, and further in-depth exploration and investigation are needed.

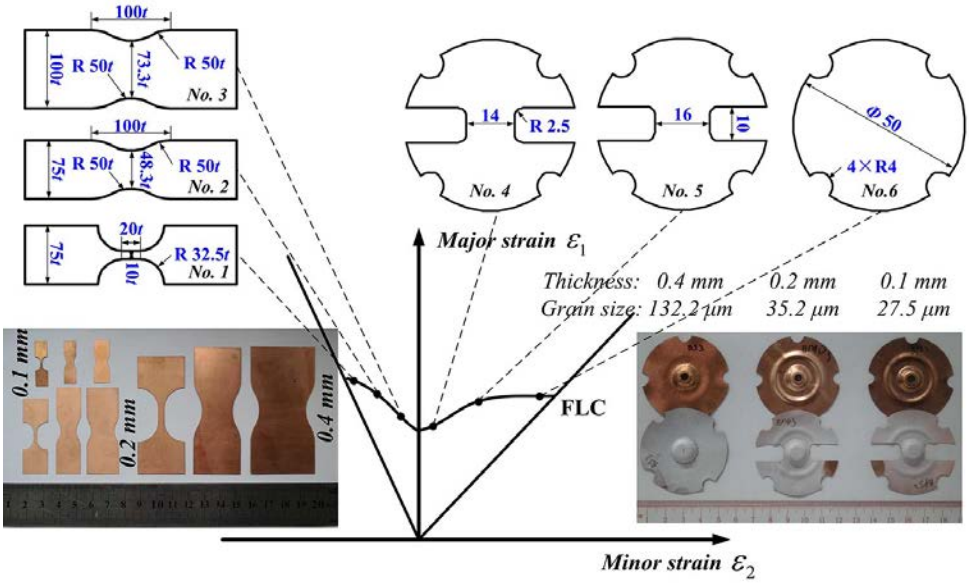

Fig. 47. Specimen designs for different uniaxial to biaxial deformation paths [125].

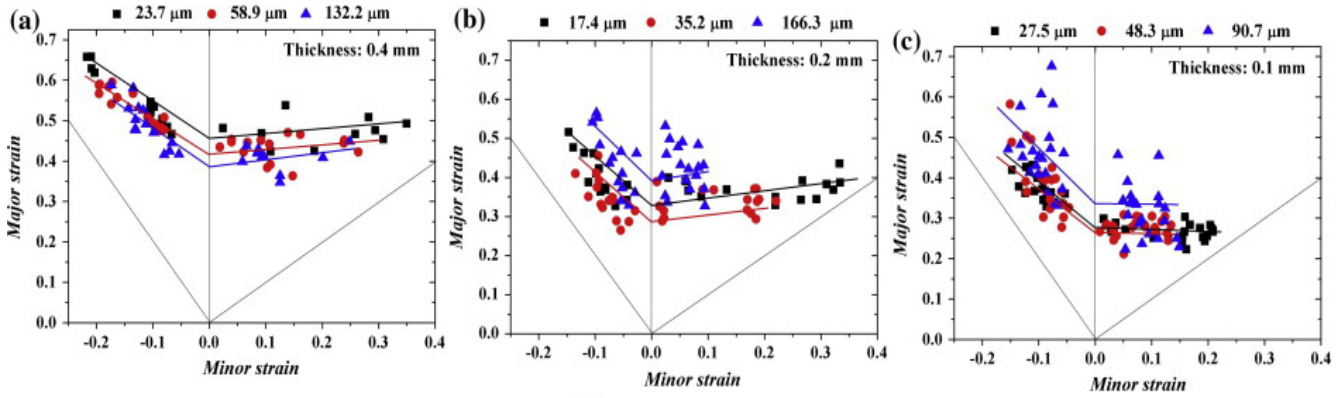

Fig. 48. FLDs of the samples with different thicknesses and grain sizes: (a) t=0.4, (b) t=0.2, and (c) t=0.1 mm [125].

6. Concluding remarks and outstanding research issues

The well-established knowledge in m-scale deformation cannot be applied directly to the forming processes at μ-scale due to the occurrence of the so-called SEs. The present review introduces the general fundamental theory of the SE and the extensive overview of the SE observations reported in the literature, followed by the detailed discussion of the underlying physical mechanisms and modeling approaches. The influence of the phenomena related to SEs on the performance of μ-scale deformation processing and the quality of μ-formed products are also reviewed comprehensively. Outstanding research issues related to SEs are identified and highlighted for further exploration and study.

In summary, SEs related phenomena arise from the interaction and transition between different deformation mechanisms that affect such parameters of the forming process as the required load, overall flow stress, critical limits for the occurrence of fracture and tearing, material flow behavior and defects distribution and patterning, friction behavior and surface roughening. In μ-scale deformation processing, these parameters are influenced by different types of SEs that dominate at different size scales. The overall underlying causes concern the inhomogeneity and anisotropy of material structure, property and deformation distribution.

Grain size and orientation can exert a very significant influence on the forming process when specimen dimensions become comparable to the grain size. This is immediately evident from the strong dependence of single crystal elastic and plastic deformation properties on the lattice orientation that may lead to differences in stiffness and strength. The onset of the associated SE is governed by the ratio of sample thickness to grain size, t/d.

A further distinct, but related group of phenomena related to the SE are associated with the presence of strain gradient within μ-forming workpieces, both due to the grain microstructure, and the shape of punch and die used e.g. for sheet forming. The peculiarity of plastic deformation in metals mediated by dislocation generation and motion is manifested in the evolution of

geometrically necessary dislocations (GND's) that govern the accommodation of non-uniform plastic flow patterns, and induce additional hardening. The characteristic length scale in strain gradient plasticity is denoted by l and depends *both* on the material, and its deformation history.

The effects of pre-existing surface roughness, variations in the frictional behavior and the evolution of roughness during forming constitute another group of SEs associated with the characteristic length scale determined by a roughness parameter (e.g. R_a) and expressed in a dimensional quantity r.

Following the overview of reported experimental results, modeling approaches were introduced to the numerical description of the underlying deformation mechanisms and the corresponding SEs. It is found that the models proposed by different authors commonly have specific application range, with no single modeling approach being able to describe accurately all manifestations of SEs in μ-scale deformation processing. The surface layer model based on an empirical "rule-of-mixtures" formula for the overall flow stress dependence on the feature and grain size provides a starting point for many further adaptations and modifications. The model predictions generally show a good match with the experimental data, although a typical limitation of this model lies in the fact that the properties of surface grains need to be calibrated, e.g. from additional experiments. The composite-based model has the similar merits of general agreement in many cases and demerits of limited applicability. For frictional SEs, cases involving lubricated forming could generally be explained adequately using the lubricant pocket model. However, in the case of dry friction achieving this level of clarity remains a challenge.

The authors are of the opinion that the adoption of modern sophisticated, physically based crystal plasticity numerical models [126] holds the greatest promise for elucidating, quantifying and controlling the uncertainties introduced into μ-forming by the SEs related to grain size, strain gradient and tribological phenomena. In order to enable the application of such modeling, detailed information about the grain morphology and orientation within the workpiece is required. This requires employing modern characterization techniques based on diffraction of electrons (EBSD)

and X-rays (e.g. μ-beam Laue), and advancing these techniques towards the ultimate goal of non-destructive three-dimensional characterization, such as has been demonstrated by Loue Orientation Tomography (LOT) [127]. Finally, further developments are needed in the area of control over the grain size and orientation of stock material. In this context significant role can be played by thermo-mechanical deformation processing of billets to induce the desired texture in combination with advanced pre-machining methods.

In the final section of the review report, the most important aspects of the SE on the overall performance of μ-scale deformation are summarized. SEs lead to a significant scatter of the load required for deformation, as well as the dimensional accuracy and quality of μ-formed parts due to single grains playing an increasingly important role in the deformation process. This is confirmed by the observation that the spatial distribution of hardness within the formed work pieces is strongly dependent on the deformed state and history of individual grains. The formability limits observed at the μ-scale differ significantly from their macroscopic counterparts, with the forming limit curve shifting down with the decreasing ratio of thickness to grain size, t/d, when t is much larger than d; however, the scatter in the forming limit curve becoming much greater when only one or two grains span the workpiece thickness.

Based on the above extensive review and analysis we list some outstanding research questions that in the authors' belief need to be fully addressed in a systematic way to provide further underpinning support for widespread industrial use of μ-manufacturing processing.

A: Mechanisms of SE

Phenomenological descriptions of SEs from different sources have been identified in different formats of μ-scale deformation. However, the unified approach proposed in this review has not yet been applied systematically to different instances of μ-scale deformation.

B: Experimental investigation of mechanism interaction

There is a lack of systematic experimental investigation of the interaction and interplay of SEs

arising from different sources. A particularly interesting and promising approach is the use of *in situ* observation techniques in close combination with simulation and modelling methods.

C: SE phenomena

SE phenomena manifest in various μ-scale deformation processes include flow irregularity, frictional change, flow stress variation, variations in the fracture behavior, etc. These instances of SE-affected behavior cause scatter in the performance in μ-scale deformation.

D: Modeling and simulation of SEs

The surface layer model and composite model summarized in this review are at present the most popular constitutive modeling approaches. There is a great need for further work using the crystal plasticity modelling approach, with proper account taken of the dislocation density and related parameters for modeling SEs. The most critical issue for these models is the accurate determination of model parameters. To this end, experimental data interpretation needs to be conducted at the appropriate scale and resolution, to refine physically based constitutive models that capture correctly the deformation mode, stress distribution, dislocation substructure evolution.

E: Knowledge transfer from m-scale to μ-scale domain

The well established knowledge base in m-scale deformation is largely heuristic. The transfer of this methodology to the μ-scale is fraught with problems due to the SE, since classical trends such as the Hall-Petch relation become modified or violated with the change of scale. Therefore, the transition from the m-scale to μ-scale must be accomplished not purely on the mechanistic, but rather on the physical basis.

F: Controlling and reducing performance scatter and uncertainty

The increased level of uncertainty in μ-scale deformation is associated with lacunae in characterization. Where at the m-scale the overall statistical measures such as the average grain size and its distribution, overall texture etc. suffice for the purpose of predicting deformation behavior, at the μ-scale the small number statistics prevail, requiring a different level of detail in the workpiece microstructural control and characterization to reduce scatter. This critical issue

affects practical mass production of μ-scale parts and components. The two fundamental approaches open in this regard are either (i) refining the grain to the nano-scale and beyond, e.g. making use of bulk metallic glass, and (ii) identifying and employing novel characterization tools that combine efficiency and ease of access with suitable sensitivity.

Acknowledgements

M.W. Fu would like to thank the funding support to this research from the project BQ33F of the General Research Fund, the projects of G-UA8U, G-YBDM and G-YBL2 from The Hong Kong Polytechnic University, and the project of No. 51575465 from the National Natural Science Foundation of China.

AMK acknowledges funding received for the MBLEM laboratory at Oxford through EU FP7 project iSTRESS (604646), and access to the facilities at the Research Complex at Harwell (RCaH) via the Centre for In situ Processing Studies (CIPS).

References

[1] Kupka RK, Bouamrane F, Cremers C, Megtert S. Microfabrication: LIGA-X and applications. Appl Surf Sci. 2000;164:97-110.

[2] Malek CK, Saile V. Applications of LIGA technology to precision manufacturing of high-aspect-ratio micro-components and -systems: a review. Microelectron J. 2004;35:131-43.

[3] de Gans BJ, Duineveld PC, Schubert US. Inkjet printing of polymers: state of the art and future developments. Adv Mater. 2004;16:203-13.

[4] Masuzawa T. State of the Art of Micromachining. CIRP Annals - Manufacturing Technology. 2000;49:473-88.

[5] Dornfeld D, Min S, Takeuchi Y. Recent Advances in Mechanical Micromachining. CIRP Annals - Manufacturing Technology. 2006;55:745-68.

[6] Heckele M, Schomburg W. Review on micro molding of thermoplastic polymers. J Micromech Microeng. 2003;14:R1.

[7] Giboz J, Copponnex T, Mélé P. Microinjection molding of thermoplastic polymers: a review. J Micromech Microeng. 2007;17:R96.

[8] Giboz J, Copponnex T, Mélé P. Microinjection molding of thermoplastic polymers: morphological comparison with conventional injection molding. J Micromech Microeng. 2009;19:025023.

[9] Liu ZY, Loh NH, Tor SB, Khor KA, Murakoshi Y, Maeda R, et al. Micro-powder injection molding. J Mater Process Technol. 2002;127:165-8.

[10] Zauner R. Micro powder injection moulding. Microelectron Eng. 2006;83:1442-4.

[11] Engel U, Eckstein R. Microforming - from basic research to its realization. J Mater Process Technol. 2002;125:35-44.

[12] Vollertsen F, Niehoff HS, Hu Z. State of the art in micro forming. International Journal of Machine Tools and Manufacture. 2006;46:1172-9.

[13] Fu MW, Chan WL. A review on the state-of-the-art microforming technologies. Int J Adv Manuf Tech. 2013;67:2411-37.

[14] Geiger M, Kleiner M, Eckstein R, Tiesler N, Engel U. Microforming. CIRP Annals - Manufacturing Technology. 2001;50:445-62.

[15] Chan WL, Fu MW, Lu J, Chan LC. Simulation-enabled study of folding defect formation and avoidance in axisymmetrical flanged components. J Mater Process Technol. 2009;209:5077-86.

[16] Chan WL, Fu MW, Lu J. FE Simulation-Based Folding Defect Prediction and Avoidance in Forging of Axially Symmetrical Flanged Components. J Manuf Sci E-T Asme. 2010;132.

[17] Messner A, Engel U, Kals R, Vollertsen F. Size effect in the FE-simulation of micro-forming processes. J Mater Process Technol. 1994;45:371-6.

[18] Vollertsen F, Hu Z, Niehoff HS, Theiler C. State of the art in micro forming and investigations into micro deep drawing. J Mater Process Technol. 2004;151:70-9.

[19] Vollertsen F, Biermann D, Hansen HN, Jawahir I, Kuzman K. Size effects in manufacturing of metallic components. CIRP Annals-Manufacturing Technology. 2009;58:566-87.

[20] Diehl A, Engel U, Geiger M. Influence of microstructure on the mechanical properties and the forming behaviour of very thin metal foils. Int J Adv Manuf Tech. 2010;47:53-61.

[21] Chan WL, Fu MW, Lu J, Liu JG. Modeling of grain size effect on micro deformation behavior in micro-forming of pure copper. Mat Sci Eng a-Struct. 2010;527:6638-48.

[22] Weiss B, Gröger V, Khatibi G, Kotas A, Zimprich P, Stickler R, et al. Characterization of mechanical and thermal properties of thin Cu foils and wires. Sensors and Actuators A: Physical. 2002;99:172-82.
[23] Khatibi G, Mingler B, Schafler E, Stickler R, Weiss B. Microcharacterization of thin copper and aluminium bond wires. BHM Berg-und Hüttenmännische Monatshefte. 2005;150:176-80.
[24] Khatibi G, BETZWAR‐KOTAS A, Gröger V, Weiss B. A study of the mechanical and fatigue properties of metallic microwires. Fatigue & Fracture of Engineering Materials & Structures. 2005;28:723-33.
[25] Simons G, Weippert C, Dual J, Villain J. Size effects in tensile testing of thin cold rolled and annealed Cu foils. Mater Sci Eng, A. 2006;416:290-9.
[26] Fu MW, Chan WL. Geometry and grain size effects on the fracture behavior of sheet metal in micro-scale plastic deformation. Mater Design. 2011;32:4738-46.
[27] Ran JQ, Fu MW, Chan WL. The influence of size effect on the ductile fracture in micro-scaled plastic deformation. Int J Plast. 2013;41:65-81.
[28] Eichenhueller B, Egerer E, Engel U. Microforming at elevated temperature-forming and material behaviour. Int J Adv Manuf Technol. 2007;33:119-24.
[29] Gau JT, Principe C, Yu M. Springback behavior of brass in micro sheet forming. J Mater Process Technol. 2007;191:7-10.
[30] Liu JG, Fu MW, Lu J, Chan WL. Influence of size effect on the springback of sheet metal foils in micro-bending. Comput Mater Sci. 2011;50:2604-14.
[31] Wang JL, Fu MW, Ran JQ. Analysis of the Size Effect on Springback Behavior in Micro-Scaled U-Bending Process of Sheet Metals. Adv Eng Mater. 2014;16:421-32.
[32] Engel U. Tribology in microforming. Wear. 2006;260:265-73.
[33] Chan WL, Fu MW, Yang B. Experimental studies of the size effect affected microscale plastic deformation in micro upsetting process. Mater Sci Eng, A. 2012;534:374-83.
[34] Chan W, Fu M. Experimental and simulation based study on micro-scaled sheet metal deformation behavior in microembossing process. Mater Sci Eng, A. 2012;556:60-7.
[35] Chan W, Fu M. Experimental studies of plastic deformation behaviors in microheading process. J Mater Process Technol. 2012;212:1501-12.
[36] Egerer E, Engel U. Process characterization and material flow in microforming at elevated temperatures. Journal of manufacturing processes. 2004;6:1-6.
[37] Rosochowski A, PreSE W, Olejnik L, Richert M. Micro-extrusion of ultra-fine grained aluminium. Int J Adv Manuf Technol. 2007;33:137-46.
[38] Geiger M, Vollertsen F, Kals R. Fundamentals on the manufacturing of sheet metal microparts. CIRP Annals-Manufacturing Technology. 1996;45:277-82.
[39] Lai X, Peng L, Hu P, Lan S, Ni J. Material behavior modelling in micro/meso-scale forming process with considering size/scale effects. Comput Mater Sci. 2008;43:1003-9.
[40] Meyers MA, Ashworth E. A Model for the Effect of Grain-Size on the Yield Stress of Metals. Philos Mag A. 1982;46:737-59.
[41] Liu JG, Fu MW, Chan WL. A constitutive model for modeling of the deformation behavior in microforming with a consideration of grain boundary strengthening. Comput Mater Sci. 2012;55:85-94.
[42] Fu M, Chan K, Lee W, Chan L. Springback in the roller forming of integrated circuit leadframes. J Mater Process Technol. 1997;66:107-11.

[43] Chen C-C, Jiang C-P. Grain size effect in the micro-V-bending process of thin metal sheets. Mater Manuf Processes. 2011;26:78-83.
[44] Joo B, Oh S, Son Y. Forming of micro channels with ultra thin metal foils. CIRP Annals-Manufacturing Technology. 2004;53:243-6.
[45] Mirzai MA, Manabe K-i, Mabuchi T. Deformation characteristics of microtubes in flaring test. J Mater Process Technol. 2008;201:214-9.
[46] Wang JL, Fu MW, Ran JQ. Analysis and avoidance of flow-induced defects in meso-forming process: simulation and experiment. Int J Adv Manuf Technol. 2013;68:1551-64.
[47] Wang JL, Fu MW, Ran JQ. Analysis of size effect on flow-induced defect in micro-scaled forming process. Int J Adv Manuf Technol. 2014;73:1475-84.
[48] Parasiz SA, Kinsey B, Krishnan N, Cao J, Li M. Investigation of deformation size effects during microextrusion. Journal of Manufacturing Science and Engineering. 2007;129:690-7.
[49] Parasiz SA, VanBenthysen R, Kinsey BL. Deformation size effects due to specimen and grain size in microbending. Journal of manufacturing science and engineering. 2010;132:011018.
[50] Manabe K, Shimizu T, Koyama H, Yang M, Ito K. Validation of FE simulation based on surface roughness model in micro-deep drawing. J Mater Process Technol. 2008;204:89-93.
[51] Wang C-J, Bin G, Shan D-B. Effect of die cavity dimension on micro U deep drawing behaviour with T2 foil. T Nonferr Metal Soc. 2009;19:s790-s4.
[52] Vollertsen F. Categories of size effects. Production Engineering. 2008;2:377-83.
[53] Bažant Z. Scaling of Structural Strength. Hermes Penton Science, London, 2nd updated ed. elsevier édition. 2002;56:62.
[54] Korsunsky AM. Power Law Multi-Scaling of Material Strength. arXiv preprint cond-mat/0508653. 2005.
[55] Ashby M. The deformation of plastically non-homogeneous materials. Philos Mag. 1970;21:399-424.
[56] Kim G-Y, Ni J, Koç M. Modeling of the size effects on the behavior of metals in microscale deformation processes. Journal of Manufacturing Science and Engineering. 2007;129:470-6.
[57] Chan WL, Fu MW, Lu J. The size effect on micro deformation behaviour in micro-scale plastic deformation. Mater Des. 2011;32:198-206.
[58] Fu MW, Chan WL. Micro-scaled Products Development via Microforming: Springer; 2014.
[59] Geiger M, Messner A, Engel U. Production of microparts—size effects in bulk metal forming, similarity theory. Production Engineering. 1997;4:55-8.
[60] Raulea L, Govaert L, Baaijens F. Grain and specimen size effects in processing metal sheets. Advanced Technology of Plasticity. 1999;2:19-24.
[61] Chen F-K, Tsai J-W. A study of size effect in micro-forming with micro-hardness tests. J Mater Process Technol. 2006;177:146-9.
[62] Barbier C, Thibaud S, Richard F, Picart P. Size effects on material behavior in microforming. Int J Mater Form. 2009;2:625-8.
[63] Chan WL, Fu MW. Studies of the interactive effect of specimen and grain sizes on the plastic deformation behavior in microforming. Int J Adv Manuf Tech. 2012;62:989-1000.
[64] Chan WL, Fu MW. Experimental studies and numerical modeling of the specimen and grain size effects on the flow stress of sheet metal in microforming. Mat Sci Eng a-Struct. 2011;528:7674-83.
[65] Hansen N. The effect of grain size and strain on the tensile flow stress of aluminium at

room temperature. Acta Metall. 1977;25:863-9.
[66] Klein M, Hadrboletz A, Weiss B, Khatibi G. The ‘size effect’on the stress–strain, fatigue and fracture properties of thin metallic foils. Mater Sci Eng, A. 2001;319:924-8.
[67] Ghobrial M, Lee J, Altan T, Bay N, Hansen B. Factors affecting the double cup extrusion test for evaluation of friction in cold and warm forging. CIRP Annals-Manufacturing Technology. 1993;42:347-51.
[68] Barcellona A, Cannizzaro L, Forcellese A, Gabrielli F. Validation of frictional studies by double-cup extrusion tests in cold-forming. CIRP Annals-Manufacturing Technology. 1996;45:211-4.
[69] Tan X, Bay N, Zhang W. On parameters affecting metal flow and friction in the double cup extrusion test. Scand J Metall. 1998;27:246-52.
[70] Mori LF, Krishnan N, Cao J, Espinosa HD. Study of the size effects and friction conditions in microextrusion—part II: size effect in dynamic friction for brass-steel pairs. Journal of Manufacturing Science and Engineering. 2007;129:677-89.
[71] Geiger M. Desgin of micro-forming processes-fundamentals material data and friction behaviour. 1995.
[72] Zhuang W, Lin J. An integrated micromechanics modelling approach for micro-forming simulation. Int J Mod Phys B. 2008;22:5907-12.
[73] OsAKADA K, OYANE M. On the roughening of free surface in deformation processes. Bulletin of JSME. 1971;14:171-7.
[74] Barlow C, Bay B, Hansen N. A comparative investigation of surface relief structures and dislocation microstructures in cold-rolled aluminium. Philosophical magazine A Physics of condensed matter Defects and mechanical properties. 1985;51:253-75.
[75] Urie V, Wain H. Plastic deformation of coarse-grained aluminium. J Inst Metals. 1952;81.
[76] Wilson D, Roberts W, Rodrigues P. Effects of grain anisotropy on limit strains in biaxial stretching: part ii. sheets of cubic metals and alloys with well-developed preferred orientations. Metall Trans A. 1981;12:1603-11.
[77] Beaudoin A, Acharya A, Chen S, Korzekwa D, Stout M. Consideration of grain-size effect and kinetics in the plastic deformation of metal polycrystals. Acta Mater. 2000;48:3409-23.
[78] Hurley P, Humphreys F. The application of EBSD to the study of substructural development in a cold rolled single-phase aluminium alloy. Acta Mater. 2003;51:1087-102.
[79] Wu P, Lloyd D. Analysis of surface roughening in AA6111 automotive sheet. Acta Mater. 2004;52:1785-98.
[80] Shi Y, Zhao P, Jin H, Wu P, Lloyd D. Analysis of Surface Roughening in AA6111 Automotive Sheet Under Pure Bending. Metallurgical and Materials Transactions A. 2016;47:949-60.
[81] Guangnan C, Huan S, Shiguang H, Baudelet B. Roughening of the free surfaces of metallic sheets during stretch forming. Mater Sci Eng, A. 1990;128:33-8.
[82] Chandrasekaran D, Nygårds M. A study of the surface deformation behaviour at grain boundaries in an ultra-low-carbon steel. Acta Mater. 2003;51:5375-84.
[83] Meng B, Fu MW. Size effect on deformation behavior and ductile fracture in microforming of pure copper sheets considering free surface roughening. Mater Design. 2015;83:400-12.
[84] Miyazaki S, Shibata K, Fujita H. Effect of specimen thickness on mechanical properties of polycrystalline aggregates with various grain sizes. Acta Metall. 1979;27:855-62.
[85] Murr L, Hecker S. Quantitative evidence for dislocation emission from grain boundaries.

Scripta Metallurgica. 1979;13:167-71.
[86] Hug E, Keller C. Intrinsic effects due to the reduction of thickness on the mechanical behavior of nickel polycrystals. Metallurgical and Materials Transactions A. 2010;41:2498-506.
[87] Yu S, Yu H-P, Ruan X-Y. Discussion and prediction on decreasing flow stress scale effect. T Nonferr Metal Soc. 2006;16:132-6.
[88] Peng LF, Liu F, Ni J, Lai XM. Size effects in thin sheet metal forming and its elastic-plastic constitutive model. Mater Design. 2007;28:1731-6.
[89] Armstrong R, Codd I, Douthwaite R, Petch N. The plastic deformation of polycrystalline aggregates. Philos Mag. 1962;7:45-58.
[90] Armstrong R. On size effects in polycrystal plasticity. Journal of the Mechanics and Physics of Solids. 1961;9:196-9.
[91] Peng L, Lai X, Lee H-J, Song J-H, Ni J. Analysis of micro/mesoscale sheet forming process with uniform size dependent material constitutive model. Mater Sci Eng, A. 2009;526:93-9.
[92] Hansen N. Polycrystalline strengthening. Metall Trans A. 1985;16:2167-90.
[93] Jiang Z, Lian J, Baudelet B. A dislocation density approximation for the flow stress—grain size relation of polycrystals. Acta metallurgica et materialia. 1995;43:3349-60.
[94] Fu HH, Benson DJ, Meyers MA. Analytical and computational description of effect of grain size on yield stress of metals. Acta Mater. 2001;49:2567-82.
[95] Argon AS. Strengthening mechanisms in crystal plasticity: Oxford University Press; 2008.
[96] Zhao M, Slaughter WS, Li M, Mao SX. Material-length-scale-controlled nanoindentation size effects due to strain-gradient plasticity. Acta Mater. 2003;51:4461-9.
[97] Nix WD, Gao H. Indentation size effects in crystalline materials: a law for strain gradient plasticity. Journal of the Mechanics and Physics of Solids. 1998;46:411-25.
[98] Michel J-F, Picart P. Modelling the constitutive behaviour of thin metal sheet using strain gradient theory. J Mater Process Technol. 2002;125:164-9.
[99] Ran JQ, Fu MW. A hybrid model for analysis of ductile fracture in micro-scaled plastic deformation of multiphase alloys. Int J Plast. 2014;61:1-16.
[100] Wang S, Zhuang W, Balint D, Lin J. A virtual crystal plasticity simulation tool for micro-forming. Procedia Engineering. 2009;1:75-8.
[101] Zhuang W, Wang S, Cao J, Lin J, Hartl C. Modelling of localised thinning features in the hydroforming of micro-tubes using the crystal-plasticity FE method. Int J Adv Manuf Technol. 2010;47:859-65.
[102] Deng JH, Fu MW, Chan WL. Size effect on material surface deformation behavior in micro-forming process. Mater Sci Eng, A. 2011;528:4799-806.
[103] Tiesler N. Microforming-size effects in friction and their influence on extrusion processes. Wire. 2002;52:34-8.
[104] Peng L, Lai X, Lee H-J, Song J-H, Ni J. Friction behavior modeling and analysis in micro/meso scale metal forming process. Mater Design. 2010;31:1953-61.
[105] Yeh F-H, Li C-L, Lu Y-H. Study of thickness and grain size effects on material behavior in micro-forming. J Mater Process Technol. 2008;201:237-41.
[106] Hall EO. The Deformation and Ageing of Mild Steel: III Discussion of Results. Proceedings of the Physical Society Section B. 1951;64:747.
[107] Petch NJ. The Cleavage Strength of Polycrystals. J Iron Steel Inst. 1953;174:25-8.
[108] Pijaudier‐Cabot G, Bažant Z. Nonlocal Damage Theory. Journal of Engineering

Mechanics. 1987;113:1512-33.
[109] Fu MW, Yang B, Chan WL. Experimental and simulation studies of micro blanking and deep drawing compound process using copper sheet. J Mater Process Technol. 2013;213:101-10.
[110] Geißdörfer S, Rosochowski A, Olejnik L, Engel U, Richert M. Micro-extrusion of ultrafine grained copper. Int J Mater Form. 2008;1:455-8.
[111] Krishnan N, Cao J, Dohda K. Study of the size effect on friction conditions in microextrusion—part I: microextrusion experiments and analysis. Journal of Manufacturing Science and Engineering. 2007;129:669-76.
[112] Meng B, Fu MW, Fu CM, Chen KS. Ductile fracture and deformation behavior in progressive microforming. Mater Design. 2015;83:14-25.
[113] Diehl A, Engel U, Geiger M. Mechanical properties and bending behaviour of metal foils. Proceedings of the Institution of Mechanical Engineers Part B Journal of engineering manufacture 2008;222:83-91.
[114] Diehl A, Engel U, Geiger M. Spring-back behaviour of thin metal foils in free bending processes. Multi-Material Micro Manufacture. 2005:147-50.
[115] Meng B, Fu MW, Fu CM, Wang JL. Multivariable analysis of micro shearing process customized for progressive forming of micro-parts. International Journal of Mechanical Sciences. 2015;93:191-203.
[116] Chan WL, Fu MW. Meso-scaled progressive forming of bulk cylindrical and flanged parts using sheet metal. Mater Design. 2013;43:249-57.
[117] Hall E. Variation of hardness of metals with grain size. 1954.
[118] Farhat ZN, Ding Y, Northwood DO, Alpas AT. Effect of grain size on friction and wear of nanocrystalline aluminum. Mater Sci Eng, A. 1996;206:302-13.
[119] Gau J-T, Principe C, Wang J. An experimental study on size effects on flow stress and formability of aluminm and brass for microforming.J Mater Process Technol. 2007;184:42-6.
[120] Raulea L, Goijaerts A, Govaert L, Baaijens F. Size effects in the processing of thin metal sheets. J Mater Process Technol. 2001;115:44-8.
[121] Michel J-F, Picart P. Size effects on the constitutive behaviour for brass in sheet metal forming. J Mater Process Technol. 2003;141:439-46.
[122] Diehl A, Staud D, Engel U. Investigation of the mechanical behaviour of thin metal sheets using the hydraulic bulge test. 4th International Conference on Multi-Material Micro Manufacture, Cardiff, Wales, UK 2008. p. 195-8.
[123] Xu ZT, Peng LF, Lai XM, Fu MW. Geometry and grain size effects on the forming limit of sheet metals in micro-scaled plastic deformation. Mater Sci Eng, A. 2014;611:345-53.
[124] Pan B. Recent progress in digital image correlation. Experimental Mechanics. 2011;51:1223-35.
[125] Xu ZT, Peng LF, Fu MW, Lai XM. Size effect affected formability of sheet metals in micro/meso scale plastic deformation: Experiment and modeling. Int J Plast. 2015;68:34-54.
[126] Song X, Hofmann F, Korsunsky AM. Dislocation-based plasticity model and micro-beam Laue diffraction analysis of polycrystalline Ni foil: A forward prediction. Philos Mag. 2010;90:3999-4011.
[127] Hofmann F, Keegan S, Korsunsky AM. Diffraction post-processing of 3D dislocation dynamics simulations for direct comparison with micro-beam Laue experiments. Mater Lett. 2012;89:66-9.